ORIGINAL PAPER

New third-order convex splitting methods and analysis for the phase field crystal equation

Zhijian Ye[1] · Zhoushun Zheng[1] · Zhilin Li[2]

Abstract

In this paper, three new third-order accurate schemes are proposed and analyzed for the phase field crystal equation modeled by the Swift-Hohenberg energy functional with periodic boundary conditions based on three types of convex splittings. Firstly, using a third-order backward differentiation formula for the temporal discretization, we treat the convex and concave parts produced by the energy splitting implicitly and explicitly, respectively. Next, we develop three nonlinear third-order semi-discrete schemes and present rigorous proofs of the mass conservation, unique solvability, and the energy stability. The Fourier pseudo-spectral method is utilized for the spatial discretization and some advanced nonlinear iterative solvers are applied to solve the discrete system. Furthermore, various numerical experiments in two and three dimensional are presented to demonstrate the accuracy, energy stability, and mass conservation of the proposed schemes.

Keywords Phase field crystal equation · Convex splitting method · Third-order backward difference formula · Unique solvability · Energy stability

✉ Zhoushun Zheng
zszheng@csu.edu.cn

Zhijian Ye
yezj577@163.com

Zhilin Li
zhilin@math.ncsu.edu

1   School of Mathematics and Statistics, Central South University, Changsha 410083, Hunan, China

2   CRSC & Department of Mathematics, North Carolina State University, Raleigh 27695-8205, NC, USA

🙂 Springer

1 Introduction

The phase field crystal (PFC) model proposed by Elder et al. [1, 2] has been frequently used to simulate the microstructural evolution of crystal growth on atomic length and diffusive time scales. The PFC model can nucleate crystallites at arbitrary locations and orientations and contain elastic and plastic deformations. At present, the PFC model has been successfully applied to simulate many physical phenomena, including grain boundary structures, elastic and plastic deformations of crystals, crystal growth in a supercooled liquid, dendritic and eutectic solidification, and epitaxial thin film growth, see, for example, [2–6].

It is challenging to develop efficient, stable, and structure-preserving numerical schemes for solving the PFC equation due to high-order spacial derivatives and its nonlinearity. There are various numerical schemes proposed for solving the PFC equation in recent decades. At first, Elder et al. [1, 2] applied an explicit Euler scheme for solving the PFC equation, which is simple and easy to implement. However, the explicit Euler scheme leads to severe time step restrictions, which makes long-time numerical simulations very difficult. In order to take a larger time step to solve the PFC equation more efficiently, quite a few semi-implicit methods emerged later. Backofen et al. [7] developed a first-order accurate semi-implicit discretization (in time) by linearizing the nonlinear term based on the backward Euler discretization. Backofen's scheme allows large time steps and only requires the solution of a linear system at each time step. However, rigorous energy stability analysis is lacking, *c.f.*, [7]. Cheng et al. [8] presented a first-order accurate (in time) unconditionally stable algorithm but without analysis of the energy stability to solve the PFC equation.

In recent years, based on the convex splitting (CS) method designed to solve the Cahn-Hilliard equation in [9], several first and second-order numerical schemes for the PFC equation have been proposed to overcome the time step restriction and to guarantee the energy stability. In the framework of the CS method, implicit and explicit discretization are applied to the convex and concave parts of the energy functional, respectively, which results in nonlinear schemes with the unique solvability, energy stability, and more significantly relatively large time steps. Based on the CS strategy, Wise et al. [10] presented a first order and unconditionally energy-stable finite difference scheme for the PFC equation. Using the similar CS idea as in [10], Hu et al. [11] proposed a second order, unconditionally energy-stable finite difference method to solve the PFC equation with several numerical examples to verify the energy stability of the CS method numerically. Subsequently, with the strategy of the convex splitting of energy functional, more numerical methods for the PFC equation have been developed [12–18]. In addition to the CS strategy, there are other energy-stable nonlinear schemes for solving the PFC equation, see for example, [19–23]. In particular, the methods proposed in [20–22] are fully implicit schemes with adaptive time-stepping strategies. More recently, there are some other new numerical methods for solving the PFC equation, such as invariant energy quadratization (IEQ) [24, 25], scalar auxiliary variable (SAV) approaches [26, 27], operator splitting schemes [28, 29], three-level second-order linearized difference scheme [30], and stabilized semi-implicit (SSI) methods [31].

It is worth noting that all the methods mentioned above are first- or second-order accurate in time. To capture oscillatory solutions and fine resolution of the solutions, high-order accurate numerical methods are preferred especially for long-time simulations of the PFC equation. There are few studies on temporal higher-order numerical methods for the PFC equation. We briefly described several third-order approaches for solving phase field equations. Based on the ideas of CS methods, Shin et al. [32] constructed a third-order convex splitting Runge–Kutta (CSRK) method for the PFC equation. Cheng et al. [33] proposed and analyzed a temporal third-order accurate backward difference formula (BDF) method for the Cahn-Hilliard equation. Recently, combining the third-order backward difference formula (BDF3) with the CS strategy, Zhang et al. [34] developed a third-order scheme for the two-mode PFC equation, which is similar to the PFC model studied in this paper.

It is believed that the BDF3 scheme presented in [34] is more efficient than that proposed in [32] because the latter needs to solve six nonlinear systems of equations at each time step. However, the energy stability of the BDF3 scheme constructed in [34] depends on a stabilized term needed in the method. It seems that almost all the third-order methods are all based on the convex splitting.

In this paper, we develop and analyze three third-order accurate methods based on three types of convex splittings and the BDF3 temporal approximation for the PFC equation with periodic boundary conditions. Compared with the existing third-order method [32] based on convex splitting Runge–Kutta, our method is more efficient. Note that one of the CS methods introduced in this paper has not been applied to the PFC equation. When the time step satisfies a relatively loose requirement, our proposed schemes can guarantee the energy stability without adding a stabilized term, in contrast to the third-order approach presented in [34]. The highlights of our work in this paper are summarized below.

- New third-order methods that are mass conserving and uniquely solvable through rigorous proofs.
- The new methods are rigorously proven to be energy stable under certain conditions.
- The proposed third-order temporal discretization can be easily combined with the Fourier pseudo-spectral method in the spatial discretization to obtain high-order accuracy both in time and space.
- Our new methods and analysis are validated through several numerical examples including long-time simulations.

The paper is organized as follows. The properties of the PFC equation and three types of convex splitting strategies for the energy functional of the PFC equation are introduced in Sect. 2. In Sect. 3, we present three third-order CS schemes and analysis. In Sect. 4, we discuss the implementation details. In Sect. 5, various numerical examples in two and three dimensions are presented to demonstrate the accuracy, energy stability, mass conservation, and efficiency of the proposed methods. We conclude in Sect. 6.

2 Governing systems and energy splittings

Consider the following free energy functional of Swift-Hohenberg type [35],

$$E(u) = \int_\Omega \left(\frac{1}{2}u(\mathbf{I}+\Delta)^2 u + \frac{1}{4}u^4 - \frac{\varepsilon}{2}u^2 \right) d\mathbf{x}, \tag{1}$$

where $\mathbf{x} \in \Omega \subseteq \mathbb{R}^d$ $(d = 1, 2, 3)$, the phase field variable u is the atomic density field, ε is a bifurcation constant with physical significance such that $0 < \varepsilon < 1$, $\mathbf{I}$ is the identity operator, and Δ is the Laplacian operator, satisfying $(\mathbf{I}+\Delta)^2 = \mathbf{I}+2\Delta+\Delta^2$.

According to Elder et al. [1, 2], the gradient flow associated with the free energy functional $E(u)$ describes the following initial-boundary value problem,

$$u_t = \Delta\mu, \quad \mathbf{x} \in \Omega, \ t \in (0, T], \tag{2}$$

$$\mu = \frac{\delta E}{\delta u} = (\mathbf{I}+\Delta)^2 u + u^3 - \varepsilon u, \quad \mathbf{x} \in \Omega, \ t \in (0, T], \tag{3}$$

$$u(\mathbf{x}, 0) = u_0(\mathbf{x}), \quad \mathbf{x} \in \Omega, \tag{4}$$

$$u(\mathbf{x}, t) \text{ is } \Omega\text{-periodic}, \quad t \in (0, T], \tag{5}$$

where T is the final time, μ is called the chemical potential, and $\frac{\delta E}{\delta u}$ is the variational derivative with respect to u. We impose the periodic boundary conditions (5) in this paper, with which we can easily prove that the PFC (2)–(3) is mass conservative in the sense that $\frac{d}{dt} \int_\Omega u \, d\mathbf{x} = 0$. Furthermore, we can derive that the system satisfies the following energy dissipation,

$$\frac{d}{dt} E(u) = -\|\nabla\mu\|^2 \leqslant 0,$$

where $\|\cdot\|$ denote the L^2 norm and ∇ is the gradient operator.

We first introduce some notations and definitions needed in our discussions. We use $(\cdot, \cdot)$ to denote the L^2 inner product. Thus, the L^2 norm is $\|\cdot\| = \sqrt{(\cdot, \cdot)}$. For each $s \geqslant 0$, let $(\cdot, \cdot)_{H^s}$ and $\|\cdot\|_{H^s}$ be the $H^s(\Omega)$ inner product and norm, respectively, where $H^s(\Omega)$ is the Sobolev space and $H^0(\Omega) = L^2(\Omega)$. We then define the following Sobolev spaces,

$$L_0^2(\Omega) = \left\{ v \in L^2(\Omega) \,\big|\, (v, 1) = 0 \right\},$$

$$L_{per}^2(\Omega) = \left\{ v \in L^2(\Omega) \,\big|\, v \text{ is periodic on } \partial\Omega \right\},$$

$$H_{per}^s(\Omega) = \left\{ v \in H^s(\Omega) \,\big|\, v \text{ is periodic on } \partial\Omega \right\}.$$

For an $f \in L_0^2(\Omega)$, we define $v_f \in H_{per}^s(\Omega) \cap L_0^2(\Omega)$ as the unique solution of the following periodic boundary value problem,

$$-\Delta v_f = f \text{ in } \Omega,$$

or $v_f = (-\Delta)^{-1} f$. Suppose that $f, g \in L_0^2(\Omega)$, then the $H_{per}^{-1}(\Omega)$ inner product $(\cdot, \cdot)_{-1}$ and norm $\| \cdot \|_{-1}$ are defined as

$$(f, g)_{-1} = (\nabla v_f, \nabla v_g), \quad \|f\|_{-1} = \sqrt{(f, f)_{-1}},$$

respectively, where $H_{per}^{-s}(\Omega)$ is the dual space of $H_{per}^s(\Omega)$. With the periodic boundary conditions (5), we can obtain the following identity using the integration by parts,

$$(f, g)_{-1} = \left((-\Delta)^{-1} f, g\right) = \left((-\Delta)^{-1} g, f\right) = (g, f)_{-1}. \tag{6}$$

Three convex splitting strategies

Next, we introduce three types of CS strategies of the free energy functional (1) that will be employed to construct third-order time discretizations. The first type of the energy splittings is

$$E(u) = E_{BF}^c(u) - E_{BF}^e(u), \tag{7}$$

$$E_{BF}^c(u) = \int_\Omega \left(\frac{1}{2} u (\mathbf{I} + \Delta)^2 u + \frac{1}{4} u^4\right) d\mathbf{x}, \tag{8}$$

$$E_{BF}^e(u) = \int_\Omega \frac{\varepsilon}{2} u^2 \, d\mathbf{x}, \tag{9}$$

which has been used to solve the PFC equation in [13, 14, 32]. The second type of the energy splittings is

$$E(u) = E_{DF}^c(u) - E_{DF}^e(u), \tag{10}$$

$$E_{DF}^c(u) = \int_\Omega \left(\frac{1 - \varepsilon}{2} u^2 + \frac{1}{2} (\Delta u)^2 + \frac{1}{4} u^4\right) d\mathbf{x}, \tag{11}$$

$$E_{DF}^e(u) = \int_\Omega |\nabla u|^2 \, d\mathbf{x}, \tag{12}$$

which has been widely used to design first- and second-order schemes for solving the PFC equation [10, 11, 15, 17, 18]. The third type of the energy splittings is

$$E(u) = E_{BD}^c(u) - E_{BD}^e(u), \tag{13}$$

$$E_{BD}^c(u) = \int_\Omega \left(\frac{1}{2} u^2 + \frac{1}{2} (\Delta u)^2 + \frac{1}{4} u^4\right) d\mathbf{x}, \tag{14}$$

$$E_{BD}^e(u) = \int_\Omega \left(|\nabla u|^2 + \frac{\varepsilon}{2} u^2\right) d\mathbf{x}, \tag{15}$$

which has not been reported for solving the PFC equation yet although it is similar to the previous two splitting methods. In this paper, we refer to the CS method (7),

(10), and (13) as CS_{BF}, CS_{DF}, and CS_{BD}. Note that, the functionals above E_{BF}^c, E_{BF}^e, E_{DF}^c, E_{DF}^e, E_{BD}^c, and E_{BD}^e are all convex, which can be obtained conveniently by the calculation of the second variation.

3 Analysis of the BDF3 method applied to the convex splitting of the PFC equation

In recent years, CS_{BF} (7) and CS_{DF} (10) splittings have been applied to construct several first and second-order CS schemes for the PFC equation [10, 11, 13–15, 17, 18, 32]. However, there are almost no third-order CS schemes for the PFC equation except for the CSRK methods [32] that combines the Runge–Kutta methods with the convex splitting.

We propose to use the BDF3 method to develop third-order convex splitting schemes for the PFC equation. We have developed and analyzed three BDF3 methods based on the three convex splittings, CS_{BF} (7), CS_{DF} (10), and CS_{BD} (13) in this section. The mass conservation, unconditionally unique solvability, and the energy stability of the proposed schemes all have been proved. Furthermore, we will discuss the similarities and differences of the three methods in Subsection 3.4. We start with an important lemma that is needed in the proof of the energy stability.

Lemma 1 *Let a, b, c, λ be real numbers satisfying $a, c, \lambda \geqslant 0$ and $2\sqrt{a\lambda} + b \geqslant 0$. Then, for any $u \in H_{per}^{-1}(\Omega)$, the inequality holds*

$$a \|u\|_{-1}^2 + b \|u\|^2 + c \|\Delta u\|^2 \geqslant \left(2\sqrt{2c\sqrt{a\lambda} + bc} - \lambda \right) \|\nabla u\|^2. \qquad (16)$$

Proof Adding the term $\lambda \|\nabla u\|^2$ and the term $-\lambda \|\nabla u\|^2$ to the left hand side of (16) simultaneously, we have the following identical equation,

$$\begin{aligned} a \|u\|_{-1}^2 + b \|u\|^2 + c \|\Delta u\|^2 = {} & a \|u\|_{-1}^2 + \lambda \|\nabla u\|^2 + b \|u\|^2 \\ & + c \|\Delta u\|^2 - \lambda \|\nabla u\|^2. \end{aligned} \qquad (17)$$

Utilizing the Young's and Cauchy inequalities and the identity (6), we obtain

$$\begin{aligned} a \|u\|_{-1}^2 + \lambda \|\nabla u\|^2 & \geqslant 2\sqrt{a\lambda} \|u\|_{-1} \|\nabla u\| \\ & = 2\sqrt{a\lambda} \left\| \nabla(-\Delta)^{-1} u \right\| \|\nabla u\| \\ & \geqslant 2\sqrt{a\lambda} \left(\nabla (-\Delta)^{-1} u, \nabla u \right) \\ & = 2\sqrt{a\lambda} \|u\|^2. \end{aligned} \qquad (18)$$

Substitute (18) into (17), we have

$$a\,\|u\|_{-1}^2 + b\,\|u\|^2 + c\,\|\Delta u\|^2 \geqslant \left(2\sqrt{a\lambda} + b\right)\|u\|^2 + c\,\|\Delta u\|^2 - \lambda\,\|\nabla u\|^2. \quad (19)$$

Using the Young's and Cauchy inequalities again, we obtain

$$\begin{aligned}
\left(2\sqrt{a\lambda} + b\right)\|u\|^2 + c\,\|\Delta u\|^2 &\geqslant 2\sqrt{2c\sqrt{a\lambda} + bc}\ \ \|u\|\,\|\Delta u\| \\
&\geqslant 2\sqrt{2c\sqrt{a\lambda} + bc}\ \ |(u, \Delta u)| \\
&= 2\sqrt{2c\sqrt{a\lambda} + bc}\ \ \|\nabla u\|^2. \quad (20)
\end{aligned}$$

Substitute (20) into (19), we derive the inequality (16).

3.1 The BDF3 scheme based on CS$_{BF}$

To discretize the problem in time, we let N_t be a positive integer and set the following temporal discretization,

$$\tau = T/N_t,\ \ t_n = n\tau,\ n = 0, 1, \cdots, N_t.$$

Applying the standard BDF3 discretization to the temporal derivative in the CS$_{BF}$ method (7), and treating $E_{BF}^c(u)$ implicitly and $E_{BF}^e(u)$ explicitly with an extrapolation, $i.e.$, $u^{n+1} = 3u^n - 3u^{n-1} + u^{n-2}$, we have the following third-order scheme for solving the PFC equation (2)–(3),

$$\frac{\frac{11}{6}u^{n+1} - 3u^n + \frac{3}{2}u^{n-1} - \frac{1}{3}u^{n-2}}{\tau} = \Delta\mu^{n+1}, \quad (21)$$

$$\mu^{n+1} = (\mathbf{I} + \Delta)^2 u^{n+1} + \left(u^{n+1}\right)^3 - \varepsilon\left(3u^n - 3u^{n-1} + u^{n-2}\right), \quad (22)$$

where $n = 2, 3, \cdots, N_t - 1$. We refer to the scheme (21)–(22) as BDF3-CS$_{BF}$. We prove the following mass conservation of the BDF3-CS$_{BF}$ scheme.

Theorem 1 (Mass conservation of BDF3-CS$_{BF}$) *The BDF3-CS$_{BF}$ scheme (21)–(22) is mass conserving, that is, we have $\int_\Omega u^{n+1}\,d\mathbf{x} = \int_\Omega u^n\,d\mathbf{x}$ for $n = 0, 1, \cdots, N_t - 1$ under the assumption $\int_\Omega u^2\,d\mathbf{x} = \int_\Omega u^1\,d\mathbf{x} = \int_\Omega u^0\,d\mathbf{x}$.*

Proof Taking the inner product of (21) with the identity operator $\mathbf{I}$, we have

$$\begin{aligned}
\left(\frac{\frac{11}{6}u^{n+1} - 3u^n + \frac{3}{2}u^{n-1} - \frac{1}{3}u^{n-2}}{\tau}, \mathbf{I}\right) &= \left(\Delta\mu^{n+1}, \mathbf{I}\right) \\
&= -\left(\nabla\mu^{n+1}, \nabla\mathbf{I}\right) \\
&= 0.
\end{aligned}$$

Simplifying the above equation, we have

$$\left(\frac{11}{6} \left(u^{n+1} - u^n \right) - \frac{7}{6} \left(u^n - u^{n-1} \right) + \frac{1}{3} \left(u^{n-1} - u^{n-2} \right), \mathbf{I} \right) = 0.$$

which implies

$$\int_\Omega \left(\frac{11}{6} \left(u^{n+1} - u^n \right) - \frac{7}{6} \left(u^n - u^{n-1} \right) + \frac{1}{3} \left(u^{n-1} - u^{n-2} \right) \right) \, d\mathbf{x} = 0.$$

Based on the assumption that $\int_\Omega u^2 \, d\mathbf{x} = \int_\Omega u^1 \, d\mathbf{x} = \int_\Omega u^0 \, d\mathbf{x}$, we obtain $\int_\Omega u^{n+1} \, d\mathbf{x} = \int_\Omega u^n \, d\mathbf{x}$, for $n = 2, 3, \cdots, N_t - 1$.

Next, we show the unique solvability of the BDF3-CS$_{\text{BF}}$ scheme.

Theorem 2 (Unique solvability of BDF3-CS$_{\text{BF}}$) *The BDF3-CS$_{BF}$ scheme* (21)–(22) *is uniquely solvable for any time step size $\tau > 0$.*

Proof Combining (7) and (21), the scheme (21)–(22) can be rewrite as

$$\frac{\frac{11}{6} u^{n+1} - 3u^n + \frac{3}{2} u^{n-1} - \frac{1}{3} u^{n-2}}{\tau}$$
$$= \Delta \left(\frac{\delta}{\delta u} E^c_{BF}(u) \Big|_{u=u^{n+1}} - \frac{\delta}{\delta u} E^e_{BF}(u) \Big|_{u=\tilde{u}^{n+1}} \right), \tag{23}$$

where $\tilde{u}^{n+1} = 3u^n - 3u^{n-1} + u^{n-2}$. Next, we construct a functional below,

$$F(u) = \frac{3}{11} \left\| \frac{11}{6} u - 3u^n + \frac{3}{2} u^{n-1} - \frac{1}{3} u^{n-2} \right\|_{-1}^2$$
$$+ \tau E^c_{BF}(u) - \tau \left(\frac{\delta}{\delta u} E^e_{BF}(u) \Big|_{\tilde{u}^{n+1}}, u \right). \tag{24}$$

We can conclude that u^{n+1} is the unique minimizer of F if and only if for any $v \in H^{-1}_{per}(\Omega) \cap L^2_0(\Omega)$,

$$\frac{d}{d\lambda} F(u + \lambda v) \Big|_{\lambda=0} = \left(\frac{11}{6} u - 3u^n + \frac{3}{2} u^{n-1} - \frac{1}{3} u^{n-2}, v \right)_{-1}$$
$$+ \tau \left(\frac{\delta}{\delta u} E^c_{BF}(u), v \right) - \tau \left(\frac{\delta}{\delta u} E^e_{BF}(u) \Big|_{\tilde{u}^{n+1}}, v \right)$$
$$= \left(\frac{11}{6} u - 3u^n + \frac{3}{2} u^{n-1} - \frac{1}{3} u^{n-2} \right.$$
$$\left. - \tau \Delta \left(\frac{\delta}{\delta u} E^c_{BF}(u) - \frac{\delta}{\delta u} E^e_{BF}(u) \Big|_{\tilde{u}^{n+1}} \right), v \right)_{-1}$$
$$= 0, \tag{25}$$

because the functional F is strictly convex since

$$\frac{d^2}{d\lambda^2} F(u + \lambda v)\Big|_{\lambda=0} = \frac{11}{6} \|v\|_{-1}^2 + \tau \frac{d^2}{d\lambda^2} E_{BF}^c(u + \lambda v)\Big|_{\lambda=0} \geq 0.$$

Therefore, (25) is true for any $v \in H_{per}^{-1}(\Omega) \cap L_0^2(\Omega)$ if and only if the (23) holds. Hence, minimizing the strictly convex function (24) is equivalent to solving (21)–(22), which implies that the proposed scheme (21)–(22) is uniquely solvable for any time step size $\tau > 0$.

Finally, we have the following theorem for the BDF3-CS$_{BF}$ scheme (21)–(22).

Theorem 3 (Energy stability of BDF3-CS$_{BF}$) *Assuming that the time step size τ satisfies the condition $\tau \leq S_{BF}(\varepsilon)$, then we have $\tilde{E}_{BF}^{n+1} \leq \tilde{E}_{BF}^n$ for $n = 2, 3, \cdots, N_t - 1$, that is, the BDF3-CS$_{BF}$ scheme (21)–(22) is energy stable, where $S_{BF}(\varepsilon) = \frac{45(\sqrt{1+6\varepsilon}-1)}{2(6\varepsilon-1+\sqrt{1+6\varepsilon})^2}$ is a function with respect to ε and $\tilde{E}_{BF}^n$ is the modified energy defined as*

$$\begin{aligned}
\tilde{E}_{BF}^n &= \tilde{E}_{BF}\left(u^n, u^{n-1}, u^{n-2}\right) \\
&= E(u^n) + \frac{5}{12\tau} \left\|u^n - u^{n-1}\right\|_{-1}^2 + \frac{1}{6\tau} \left\|u^n - 2u^{n-1} + u^{n-2}\right\|_{-1}^2 \\
&\quad + \frac{\varepsilon}{2} \left\|u^n - u^{n-1}\right\|^2 + \frac{\varepsilon}{2} \left\|u^n - 2u^{n-1} + u^{n-2}\right\|^2.
\end{aligned} \tag{26}$$

Proof Combining the (21) and (22), we obtain

$$\frac{\frac{11}{6}u^{n+1} - 3u^n + \frac{3}{2}u^{n-1} - \frac{1}{3}u^{n-2}}{\tau} - \Delta (\mathbf{I} + \Delta)^2 u^{n+1}$$

$$-\Delta \left(u^{n+1}\right)^3 + \varepsilon \Delta \left(3u^n - 3u^{n-1} + u^{n-2}\right) = 0. \tag{27}$$

Taking the inner product of (27) with $(-\Delta)^{-1}\left(u^{n+1} - u^n\right)$, we have

$$\begin{aligned}
&\left(\frac{\frac{11}{6}u^{n+1} - 3u^n + \frac{3}{2}u^{n-1} - \frac{1}{3}u^{n-2}}{\tau}, (-\Delta)^{-1}\left(u^{n+1} - u^n\right)\right) \\
&\quad + \left(-\Delta (\mathbf{I} + \Delta)^2 u^{n+1}, (-\Delta)^{-1}\left(u^{n+1} - u^n\right)\right) \\
&\quad + \left(-\Delta \left(u^{n+1}\right)^3, (-\Delta)^{-1}\left(u^{n+1} - u^n\right)\right) \\
&\quad + \left(\varepsilon \Delta \left(3u^n - 3u^{n-1} + u^{n-2}\right), (-\Delta)^{-1}\left(u^{n+1} - u^n\right)\right) = 0. \tag{28}
\end{aligned}$$

From the first term of (28), we further derive

$$
\left(\frac{\frac{11}{6}u^{n+1} - 3u^n + \frac{3}{2}u^{n-1} - \frac{1}{3}u^{n-2}}{\tau}, (-\Delta)^{-1}\left(u^{n+1} - u^n\right) \right)
$$

$$
= \left(\frac{\frac{11}{6}u^{n+1} - 3u^n + \frac{3}{2}u^{n-1} - \frac{1}{3}u^{n-2}}{\tau}, u^{n+1} - u^n \right)_{-1}
$$

$$
= \frac{1}{\tau}\left(u^{n+1} - u^n + \frac{5}{6}\left(u^{n+1} - 2u^n + u^{n-1}\right)\right.
$$

$$
\left. - \frac{1}{3}\left(u^n - 2u^{n-1} + u^{n-2}\right), u^{n+1} - u^n \right)_{-1}
$$

$$
= \frac{2}{3\tau}\left(u^{n+1} - u^n, u^{n+1} - u^n \right)_{-1}
$$

$$
+ \frac{5}{6\tau}\left(u^{n+1} - u^n - \left(u^n - u^{n-1}\right), u^{n+1} - u^n \right)_{-1}
$$

$$
+ \frac{1}{3\tau}\left(u^{n+1} - u^n - \left(u^n - 2u^{n-1} + u^{n-2}\right), u^{n+1} - u^n \right)_{-1}
$$

$$
= \frac{2}{3\tau}\left\| u^{n+1} - u^n \right\|_{-1}^2 + \frac{5}{12\tau}\left(\left\| u^{n+1} - u^n \right\|_{-1}^2 - \left\| u^n - u^{n-1} \right\|_{-1}^2 \right.
$$

$$
+ \left\| u^{n+1} - 2u^n + u^{n-1} \right\|_{-1}^2 \right) + \frac{1}{6\tau}\left(\left\| u^{n+1} - u^n \right\|_{-1}^2 \right.
$$

$$
- \left\| u^n - 2u^{n-1} + u^{n-2} \right\|_{-1}^2 + \left\| u^{n+1} - 2u^n + 2u^{n-1} - u^{n-2} \right\|_{-1}^2 \right)
$$

$$
= \frac{5}{12\tau}\left(\left\| u^{n+1} - u^n \right\|_{-1}^2 - \left\| u^n - u^{n-1} \right\|_{-1}^2 \right)
$$

$$
+ \frac{1}{6\tau}\left(\left\| u^{n+1} - 2u^n + u^{n-1} \right\|_{-1}^2 - \left\| u^n - 2u^{n-1} + u^{n-2} \right\|_{-1}^2 \right)
$$

$$
+ \frac{5}{6\tau}\left\| u^{n+1} - u^n \right\|_{-1}^2 + \frac{1}{4\tau}\left\| u^{n+1} - 2u^n + u^{n-1} \right\|_{-1}^2
$$

$$
+ \frac{1}{6\tau}\left\| u^{n+1} - 2u^n + 2u^{n-1} - u^{n-2} \right\|_{-1}^2. \tag{29}
$$

From the second term of (28), we know that

$$
\left(-\Delta\left(\mathbf{I} + \Delta\right)^2 u^{n+1}, (-\Delta)^{-1}\left(u^{n+1} - u^n\right) \right)
$$

$$
= \left(\left(\mathbf{I} + \Delta\right)^2 u^{n+1}, u^{n+1} - u^n \right)
$$

$$
= \left(\left(\mathbf{I} + \Delta\right) u^{n+1}, \left(\mathbf{I} + \Delta\right) u^{n+1} - \left(\mathbf{I} + \Delta\right) u^n \right)
$$

$$
= \frac{1}{2}\left\| \left(\mathbf{I} + \Delta\right) u^{n+1} \right\|^2 - \frac{1}{2}\left\| \left(\mathbf{I} + \Delta\right) u^n \right\|^2 + \frac{1}{2}\left\| \left(\mathbf{I} + \Delta\right)\left(u^{n+1} - u^n\right) \right\|^2. \tag{30}
$$

Next, from the third term of (28), we continue to derive

$$
\left(-\Delta \left(u^{n+1} \right)^3, (-\Delta)^{-1} \left(u^{n+1} - u^n \right) \right)
$$

$$
= \left(\left(u^{n+1} \right)^2, u^{n+1} \left(u^{n+1} - u^n \right) \right)
$$

$$
= \left(\left(u^{n+1} \right)^2, \frac{1}{2} \left(\left(u^{n+1} \right)^2 - (u^n)^2 + \left(u^{n+1} - u^n \right)^2 \right) \right)
$$

$$
= \frac{1}{2} \left(\left(u^{n+1} \right)^2, \left(u^{n+1} \right)^2 - (u^n)^2 \right) + \frac{1}{2} \left(\left(u^{n+1} \right)^2, \left(u^{n+1} - u^n \right)^2 \right)
$$

$$
= \frac{1}{4} \left(\left\| \left(u^{n+1} \right)^2 \right\|^2 - \left\| (u^n)^2 \right\|^2 \right) + \frac{1}{4} \left\| \left(u^{n+1} \right)^2 - (u^n)^2 \right\|^2
$$

$$
+ \frac{1}{2} \left\| u^{n+1} \left(u^{n+1} - u^n \right) \right\|^2. \tag{31}
$$

From the fourth term of (28), we further have

$$
\left(\varepsilon \Delta \left(3u^n - 3u^{n-1} + u^{n-2} \right), (-\Delta)^{-1} \left(u^{n+1} - u^n \right) \right)
$$

$$
= - \varepsilon \left(3u^n - 3u^{n-1} + u^{n-2}, u^{n+1} - u^n \right)
$$

$$
= - \varepsilon \left(u^{n+1} - \left(u^{n+1} - 2u^n + u^{n-1} \right) + \left(u^n - 2u^{n-1} + u^{n-2} \right), u^{n+1} - u^n \right)
$$

$$
= - \frac{\varepsilon}{2} \left(\left\| u^{n+1} \right\|^2 - \left\| u^n \right\|^2 \right) - \frac{\varepsilon}{2} \left\| u^{n+1} - u^n \right\|^2
$$

$$
+ \frac{\varepsilon}{2} \left(\left\| u^{n+1} - u^n \right\|^2 - \left\| u^n - u^{n-1} \right\|^2 \right) + \frac{\varepsilon}{2} \left\| u^{n+1} - 2u^n + u^{n-1} \right\|^2
$$

$$
- \varepsilon \left(u^n - 2u^{n-1} + u^{n-2}, u^{n+1} - u^n \right)
$$

$$
\geqslant - \frac{\varepsilon}{2} \left(\left\| u^{n+1} \right\|^2 - \left\| u^n \right\|^2 \right) - \frac{\varepsilon}{2} \left\| u^{n+1} - u^n \right\|^2
$$

$$
+ \frac{\varepsilon}{2} \left(\left\| u^{n+1} - u^n \right\|^2 - \left\| u^n - u^{n-1} \right\|^2 \right) + \frac{\varepsilon}{2} \left\| u^{n+1} - 2u^n + u^{n-1} \right\|^2
$$

$$
- \frac{\varepsilon}{2} \left(\left\| u^n - 2u^{n-1} + u^{n-2} \right\|^2 + \left\| u^{n+1} - u^n \right\|^2 \right)
$$

$$
= - \frac{\varepsilon}{2} \left(\left\| u^{n+1} \right\|^2 - \left\| u^n \right\|^2 \right) + \frac{\varepsilon}{2} \left(\left\| u^{n+1} - u^n \right\|^2 - \left\| u^n - u^{n-1} \right\|^2 \right)
$$

$$
+ \frac{\varepsilon}{2} \left(\left\| u^{n+1} - 2u^n + u^{n-1} \right\|^2 - \left\| u^n - 2u^{n-1} + u^{n-2} \right\|^2 \right) - \varepsilon \left\| u^{n+1} - u^n \right\|^2. \tag{32}
$$

Thus, combining (26), (28)–(32), we obtain

$$
\begin{aligned}
0 \geqslant{} & \tilde{E}_{BF}^{n+1} - \tilde{E}_{BF}^n + \frac{5}{6\tau}\left\|u^{n+1} - u^n\right\|_{-1}^2 + \frac{1}{4\tau}\left\|u^{n+1} - 2u^n + u^{n-1}\right\|_{-1}^2 \\
& + \frac{1}{6\tau}\left\|u^{n+1} - 2u^n + 2u^{n-1} - u^{n-2}\right\|_{-1}^2 + \frac{1}{2}\left\|(\mathbf{I}+\Delta)\left(u^{n+1} - u^n\right)\right\|^2 \\
& + \frac{1}{4}\left\|\left(u^{n+1}\right)^2 - \left(u^n\right)^2\right\|^2 + \frac{1}{2}\left\|u^{n+1}\left(u^{n+1} - u^n\right)\right\|^2 - \varepsilon\left\|u^{n+1} - u^n\right\|^2 \\
\geqslant{} & \tilde{E}_{BF}^{n+1} - \tilde{E}_{BF}^n + \frac{5}{6\tau}\left\|u^{n+1} - u^n\right\|_{-1}^2 + \frac{1}{2}\left\|(\mathbf{I}+\Delta)\left(u^{n+1} - u^n\right)\right\|^2 \\
& - \varepsilon\left\|u^{n+1} - u^n\right\|^2.
\end{aligned}
\tag{33}
$$

Associating (33) with the following equation,

$$
\begin{aligned}
& \frac{1}{2}\left\|(\mathbf{I}+\Delta)\left(u^{n+1} - u^n\right)\right\|^2 \\
={} & \frac{1}{2}\left(u^{n+1} - u^n + \Delta\left(u^{n+1} - u^n\right), u^{n+1} - u^n + \Delta\left(u^{n+1} - u^n\right)\right) \\
={} & \frac{1}{2}\left\|u^{n+1} - u^n\right\|^2 + \frac{1}{2}\left\|\Delta\left(u^{n+1} - u^n\right)\right\|^2 - \left\|\nabla\left(u^{n+1} - u^n\right)\right\|^2,
\end{aligned}
$$

we obtain

$$
\begin{aligned}
\tilde{E}_{BF}^{n+1} - \tilde{E}_{BF}^n + \frac{5}{6\tau}\left\|u^{n+1} - u^n\right\|_{-1}^2 + \frac{1-2\varepsilon}{2}\left\|u^{n+1} - u^n\right\|^2 \\
+ \frac{1}{2}\left\|\Delta\left(u^{n+1} - u^n\right)\right\|^2 - \left\|\nabla\left(u^{n+1} - u^n\right)\right\|^2 \leqslant 0.
\end{aligned}
\tag{34}
$$

According to Lemma 1, we have

$$
\begin{aligned}
& \frac{5}{6\tau}\left\|u^{n+1} - u^n\right\|_{-1}^2 + \frac{1-2\varepsilon}{2}\left\|u^{n+1} - u^n\right\|^2 + \frac{1}{2}\left\|\Delta\left(u^{n+1} - u^n\right)\right\|^2 \\
& \geqslant \left(\sqrt{2\sqrt{\frac{10\lambda}{3\tau}} + 1 - 2\varepsilon} - \lambda\right)\left\|\nabla\left(u^{n+1} - u^n\right)\right\|^2,
\end{aligned}
\tag{35}
$$

where $\lambda \in \mathbb{R}$ such that $\lambda > 0$, and $2\sqrt{\frac{10\lambda}{3\tau}} + 1 - 2\varepsilon \geqslant 0$. Substitute (35) into (34), we obtain

$$
\tilde{E}_{BF}^{n+1} - \tilde{E}_{BF}^n + \left(\sqrt{2\sqrt{\frac{10\lambda}{3\tau}} + 1 - 2\varepsilon} - 1 - \lambda\right)\left\|\nabla\left(u^{n+1} - u^n\right)\right\|^2 \leqslant 0.
$$

Obviously, we have $\tilde{E}_{BF}^{n+1} \leqslant \tilde{E}_{BF}^n$ if the following inequality holds,

$$\sqrt{2\sqrt{\frac{10\lambda}{3\tau} + 1} - 2\varepsilon - 1} - \lambda \geqslant 0,$$

which is equivalent to

$$\tau \leqslant \frac{40\lambda}{3\left(\lambda^2 + 2\lambda + 2\varepsilon\right)^2}.$$

We define a function $f_{BF}(\lambda, \varepsilon) = \frac{40\lambda}{3(\lambda^2 + 2\lambda + 2\varepsilon)^2}$. For any given value of ε satisfying $0 < \varepsilon < 1$, if $\tau \leqslant \max_\lambda f_{BF}(\lambda, \varepsilon)$, then we can derive $\tilde{E}_{BF}^{n+1} \leqslant \tilde{E}_{BF}^n$. We can see that $\max_\lambda f_{BF}(\lambda, \varepsilon) = f_{BF}(\lambda_{BF}^*, \varepsilon)$ for a fixed value of ε, where $\lambda_{BF}^* = \frac{\sqrt{1+6\varepsilon}-1}{3}$. Note that $f_{BF}(\lambda_{BF}^*, \varepsilon) = \frac{45(\sqrt{1+6\varepsilon}-1)}{2(6\varepsilon-1+\sqrt{1+6\varepsilon})^2} = S_{BF}(\varepsilon)$.

Thus, if the time step τ satisfying $\tau \leqslant S_{BF}(\varepsilon)$, we conclude that $\tilde{E}_{BF}^{n+1} \leqslant \tilde{E}_{BF}^n$, which completes the proof of the theorem.

3.2 The BDF3 schemes based on CS$_{DF}$

Similar to the BDF3-CS$_{BF}$ scheme (21)–(22), we have designed other third-order CS schemes based on different energy splittings including the CS_{DF} (10) and the CS_{BD} (13).

The third-order scheme based on the CS$_{DF}$ (10) for solving the PFC equation is the following,

$$\frac{\frac{11}{6}u^{n+1} - 3u^n + \frac{3}{2}u^{n-1} - \frac{1}{3}u^{n-2}}{\tau} = \Delta\mu^{n+1}, \tag{36}$$

$$\mu^{n+1} = (1-\varepsilon)u^{n+1} + \Delta^2 u^{n+1} + \left(u^{n+1}\right)^3 + 2\Delta\left(3u^n - 3u^{n-1} + u^{n-2}\right), \tag{37}$$

where $n = 2, 3, \cdots, N_t - 1$. We refer to the scheme (36)–(37) as BDF3-CS$_{DF}$. In parallel, we have proved the mass conservation, unique solvability, and energy stability of the BDF3-CS$_{DF}$ scheme (36)–(37) as follows. We skip the proof there since most of the proofs are similar to those in Theorems 1, 2, and due to the page limit. We also provide the proofs for some important theorems in the Appendix.

Theorem 4 (Mass conservation of BDF3-CS$_{DF}$) *The BDF3-C S_{DF} scheme* (36)–(37) *is mass conserving, that is, $\int_\Omega u^{n+1} \, d\mathbf{x} = \int_\Omega u^n \, d\mathbf{x}$ for $n = 0, 1, \cdots, N_t - 1$ under the assumption $\int_\Omega u^2 \, d\mathbf{x} = \int_\Omega u^1 \, d\mathbf{x} = \int_\Omega u^0 \, d\mathbf{x}$.*

Theorem 5 (Unique solvability of BDF3-CS$_{DF}$) *The BDF3-C S_{DF} scheme* (36)–(37) *is uniquely solvable for any time step size $\tau > 0$.*

Theorem 6 (Energy stability of BDF3-CS$_{DF}$) *Assuming that the time step size τ satisfies the condition $\tau \leqslant S_{DF}(\varepsilon)$, then we have $\tilde{E}_{DF}^{n+1} \leqslant \tilde{E}_{DF}^n$ for $n = 2, 3, \cdots, N_t - 1$,*

that is, the BDF3-CS$_{DF}$ scheme (36)–(37) is energy stable, where $S_{DF}(\varepsilon) = \frac{45(\sqrt{13+3\varepsilon}-2)}{2(3\varepsilon+5+2\sqrt{13+3\varepsilon})^2}$ and $\tilde{E}_{DF}^n$ is the modified energy defined as

$$
\begin{aligned}
\tilde{E}_{DF}^n &= \tilde{E}_{DF}\left(u^n, u^{n-1}, u^{n-2}\right) \\
&= E(u^n) + \frac{5}{12\tau}\left\|u^n - u^{n-1}\right\|_{-1}^2 + \frac{1}{6\tau}\left\|u^n - 2u^{n-1} + u^{n-2}\right\|_{-1}^2 \\
&\quad + \left\|\nabla\left(u^n - u^{n-1}\right)\right\|^2 + \left\|\nabla\left(u^n - 2u^{n-1} + u^{n-2}\right)\right\|^2.
\end{aligned}
\tag{38}
$$

3.3 The BDF3 schemes based on CS$_{BD}$

The third-order scheme based on the CS$_{BD}$ (13) for solving the PFC equation is the following,

$$
\frac{\frac{11}{6}u^{n+1} - 3u^n + \frac{3}{2}u^{n-1} - \frac{1}{3}u^{n-2}}{\tau} = \Delta\mu^{n+1},
\tag{39}
$$

$$
\begin{aligned}
\mu^{n+1} &= u^{n+1} + \Delta^2 u^{n+1} + \left(u^{n+1}\right)^3 - \varepsilon\left(3u^n - 3u^{n-1} + u^{n-2}\right) \\
&\quad + 2\Delta\left(3u^n - 3u^{n-1} + u^{n-2}\right),
\end{aligned}
\tag{40}
$$

where $n = 2, 3, \cdots, N_t - 1$. We refer to the scheme (39)–(40) as BDF3-CS$_{BD}$. Then, we have the following theorems.

Theorem 7 (Mass conservation of BDF3-CS$_{BD}$) *The BDF3-CS$_{BD}$ scheme (39)–(40) is mass conserving, that is, $\int_\Omega u^{n+1}\, d\mathbf{x} = \int_\Omega u^n\, d\mathbf{x}$ for $n = 0, 1, \cdots, N_t - 1$ under the assumption $\int_\Omega u^2\, d\mathbf{x} = \int_\Omega u^1\, d\mathbf{x} = \int_\Omega u^0\, d\mathbf{x}$.*

Theorem 8 (Unique solvability of BDF3-CS$_{BD}$) *The BDF3-CS$_{BD}$ scheme (39)–(40) is uniquely solvable for any time step size $\tau > 0$.*

Theorem 9 (Energy stability of BDF3-CS$_{BD}$) *Assuming that the time step size τ satisfies the condition $\tau \leqslant S_{BD}(\varepsilon)$, then we have $\tilde{E}_{BD}^{n+1} \leqslant \tilde{E}_{BD}^n$ for $n = 2, 3, \cdots, N_t - 1$, that is, the BDF3-CS$_{BD}$ scheme (39)–(40) is energy stable, where $S_{BD}(\varepsilon) = \frac{45(\sqrt{13+6\varepsilon}-2)}{2(6\varepsilon+5+2\sqrt{13+6\varepsilon})^2}$ and $\tilde{E}_{BD}^n$ is the modified energy defined as*

$$
\begin{aligned}
\tilde{E}_{BD}^n &= \tilde{E}_{BD}\left(u^n, u^{n-1}, u^{n-2}\right) \\
&= E\left(u^n\right) + \frac{5}{12\tau}\left\|u^n - u^{n-1}\right\|_{-1}^2 + \frac{1}{6\tau}\left\|u^n - 2u^{n-1} + u^{n-2}\right\|_{-1}^2 \\
&\quad + \frac{\varepsilon}{2}\left\|u^n - u^{n-1}\right\|^2 + \frac{\varepsilon}{2}\left\|u^n - 2u^{n-1} + u^{n-2}\right\|^2 + \left\|\nabla\left(u^n - u^{n-1}\right)\right\|^2 \\
&\quad + \left\|\nabla\left(u^n - 2u^{n-1} + u^{n-2}\right)\right\|^2.
\end{aligned}
\tag{41}
$$

Once again, we either skip the proofs or provide them in the Appendix.

3.4 Discussion of time step sizes of the three different BDF3 schemes

From Theorems 1, 2, 4, 5, 7, and 8, we know that the BDF3-CS$_{\text{BF}}$, BDF3-CS$_{\text{DF}}$, and BDF3-CS$_{\text{BD}}$ schemes are all mass conserving and uniquely solvable for any time step size $\tau > 0$. However, according to Theorems 3, 6, and 9, there are different conditions for the energy stability of the schemes.

From Theorem 3, we can easily obtain that

$$
\begin{aligned}
\frac{\mathrm{d}}{\mathrm{d}\varepsilon} S_{BF}(\varepsilon) &= \frac{\mathrm{d}}{\mathrm{d}\varepsilon} f_{BF}\left(\lambda_{BF}^*, \varepsilon\right) \\
&= \frac{\partial}{\partial\lambda} f_{BF}(\lambda, \varepsilon)\bigg|_{\lambda=\lambda_{BF}^*} \frac{\mathrm{d}\lambda}{\mathrm{d}\varepsilon} + \frac{\partial}{\partial\varepsilon} f_{BF}(\lambda, \varepsilon)\bigg|_{\lambda=\lambda_{BF}^*} \\
&= \frac{\partial}{\partial\varepsilon} f_{BF}(\lambda, \varepsilon)\bigg|_{\lambda=\lambda_{BF}^*} \\
&< 0,
\end{aligned}
$$

that is, $S_{BF}(\varepsilon)$ is a monotonically decreasing function with respect to ε. Similarly, it is easy to show that the $S_{DF}(\varepsilon)$ and the $S_{BD}(\varepsilon)$ are both monotonically decreasing functions. In addition, the value ranges of the three functions are listed below,

$$
0.6334 \approx S_{BF}(1) < S_{BF}(\varepsilon) < \lim_{\varepsilon \to 0} S_{BF}(\varepsilon) = +\infty,
$$

$$
0.1758 \approx S_{DF}(1) < S_{DF}(\varepsilon) < S_{DF}(0) \approx 0.2423,
$$

$$
0.1365 \approx S_{BD}(1) < S_{BD}(\varepsilon) < S_{BD}(0) \approx 0.2423.
$$

In Fig. 1, we plotted the upper bounds of time step size τ for $S_{BF}(\varepsilon)$, $S_{DF}(\varepsilon)$, and $S_{BD}(\varepsilon)$ methods against ε. From Fig. 1, we observe that the scheme BDF3-CS$_{\text{BF}}$ has a larger range of time step size that guarantees the energy stability than that for the BDF3-CS$_{\text{DF}}$ and BDF3-CS$_{\text{BD}}$ schemes, especially for the small parameter ε.
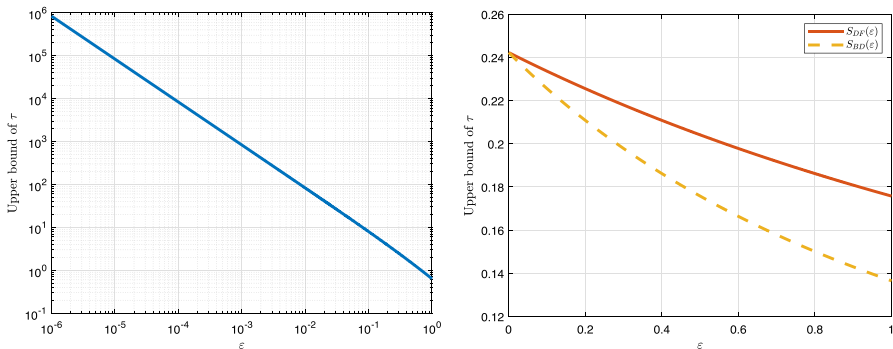
Fig. 1 Plots of the upper bounds of time step size τ for $S_{BF}(\varepsilon)$ (Left), $S_{DF}(\varepsilon)$ (Right), and $S_{BD}(\varepsilon)$ (Right) schemes against the ε

4 Spatial discretization and some implementation details

We employ the Fourier pseudo-spectral method for the spatial discretization to solve the PFC equation with periodic boundary conditions. For simplicity, we present the discussion for two-dimensional problems in this section. We have implemented the new methods for three-dimensional problems and some examples will be presented in the next section. The 3D implementation is similar to that in 2D except for an additional index.

For a 2D problem, we divide the spatial domain $\Omega = [a, a + L_x] \times [b, b + L_y]$ uniformly with the mesh size $h_x = L_x/N_x$, $h_y = L_y/N_y$ to generate the following grid,

$$\Omega_h = \big\{(x_i, y_j) \,\big|\, x_i = a + ih_x, \ y_j = b + jh_y,$$
$$0 \leqslant i \leqslant N_x - 1, \ 0 \leqslant j \leqslant N_y - 1\big\},$$

where $N_x > 1$ and $N_y > 1$ are even integers. Define a space of grid functions $V_h = \big\{u = \{u_{ij}\}, \text{ grid value at } (x_i, y_j) \in \Omega_h\big\}$ and the Fourier approximation space

$$S_N = \text{span}\Big\{e^{\mathrm{i}(\xi_k x + \eta_l y)} \,\big|\, k = -N_x/2, -N_x/2 + 1, \cdots, N_x/2 - 1,$$
$$l = -N_y/2, -N_y/2 + 1, \cdots, N_y/2 - 1\Big\},$$

where $\mathrm{i} = \sqrt{-1}$, $\xi_k = 2\pi k/L_x$, and $\eta_l = 2\pi l/L_y$. We use the following approximation

$$u(x, y) \approx u_h(x, y) = \sum_{k=-N_x/2}^{N_x/2-1} \sum_{l=-N_y/2}^{N_y/2-1} \hat{u}_{kl}\, e^{\mathrm{i}(\xi_k x + \eta_l y)}, \quad \forall u(x, y) \in L^2(\Omega), \quad (42)$$

where $\hat{u}_{kl}$ is the pseudo-spectral coefficients computed with

$$\hat{u}_{kl} = \frac{1}{N_x N_y} \sum_{i=0}^{N_x-1} \sum_{j=0}^{N_y-1} u(x_i, y_j)\, e^{-\mathrm{i}(\xi_k x_i + \eta_l y_j)}, \tag{43}$$

$k = -N_x/2, -N_x/2+1, \cdots, N_x/2-1$, and $l = -N_y/2, -N_y/2+1, \cdots, N_y/2-1$.

Let $\mathcal{F}_N$ and $\mathcal{F}_N^{-1}$ be the discrete Fourier transform and discrete inverse Fourier transform, respectively. For any grid function $u_N \in \Omega_h$, we have $\hat{u}_N = \mathcal{F}_N(u_N)$ and $u_N = \mathcal{F}_N^{-1}(\hat{u}_N)$, which can be computed from (42) and (43). The discrete Laplace operator Δ_N in terms of the Fourier transform can be expressed as

$$\Delta_N = \mathcal{F}_N^{-1}(-\Lambda)\mathcal{F}_N,$$

where $\Lambda = (\Lambda_{kl})$ and $\Lambda_{kl} = \xi_k^2 + \eta_l^2$.

Since the problem is nonlinear and the discretization is implicit, a nonlinear iterative solver for the semi-discrete scheme is needed. We employ a popular approach below, see for example, [14, 23, 28, 32, 36],

$$
\begin{aligned}
\left(u^{n+1}\right)^3 &\approx \left(u^{n,m+1}\right)^3 \\
&= (u^{n,m})^3 + 3(u^{n,m})^2(u^{n,m+1} - u^{n,m}) \\
&= 3(u^{n,m})^2 u^{n,m+1} - 2(u^{n,m})^3
\end{aligned}
$$

for $m = 0, 1, \cdots$. Thus, we have the following iterative procedure,

$$
\frac{\frac{11}{6}u^{n,m+1} - 3u^n + \frac{3}{2}u^{n-1} - \frac{1}{3}u^{n-2}}{\tau}
$$
$$
= \Delta(\mathbf{I} + \Delta)^2 u^{n,m+1} + \Delta\left(3\left(u^{n,m}\right)^2 u^{n,m+1} - 2\left(u^{n,m}\right)^3\right)
$$
$$
- \varepsilon\Delta\left(3u^n - 3u^{n-1} + u^{n-2}\right),
$$

which is the following after some simple manipulations,

$$
\left(\frac{11}{6}\mathbf{I} - \tau\Delta\left((\mathbf{I} + \Delta)^2 + 3\left(u^{n,m}\right)^2\right)\right)u^{n,m+1}
$$
$$
= 3u^n - \frac{3}{2}u^{n-1} + \frac{1}{3}u^{n-2} - 2\tau\Delta\left(u^{n,m}\right)^3 - \varepsilon\tau\Delta\left(3u^n - 3u^{n-1} + u^{n-2}\right), \quad (44)
$$

with an initial estimate $u^{n,0} = u^n$. Combining the Fourier pseudo-spectral method with the linear iterative scheme (44), we obtain the fully discrete BDF3-CS$_{\text{BF}}$ scheme, that is, assuming that u_N^{n-2}, u_N^{n-1}, and u_N^n are already computed with $n \geqslant 2$, then we update u_N^{n+1} as follows,

$$
\left(\frac{11}{6}I - \tau\Delta_N\left((I + \Delta_N)^2 + 3\left(u_N^{n,m}\right)^2\right)\right)u_N^{n,m+1}
$$
$$
= 3u_N^n - \frac{3}{2}u_N^{n-1} + \frac{1}{3}u_N^{n-2} - 2\tau\Delta_N\left(u_N^{n,m}\right)^3 - \varepsilon\tau\Delta_N\left(3u_N^n - 3u_N^{n-1} + u_N^{n-2}\right)
$$
$$
(45)
$$

for $m = 0, 1, \cdots$, with an initial estimate $u_N^{n,0} = u_N^n$, where I is the identity matrix. After the iteration convergence criterion is met, that is, $\frac{\left\|u_N^{n,m+1} - u_N^{n,m}\right\|}{\left\|u_N^{n,m}\right\|} \leqslant tol$, where tol is a given tolerance, we set $u_N^{n+1} = u_N^{n,m+1}$ and move to the next time level. At each time step, we use the generalized minimal residual (GMRES) algorithm to solver the linear system (45) with the following preconditioner P_{BF},

$$
P_{BF} = \frac{11}{6}I - \tau\Delta_N\left((I + \Delta_N)^2 + 3\overline{\left(u_N^{n,m}\right)^2}I\right),
$$

where $\overline{(\cdot)}$ denotes the average value of $(\cdot)$.

Remark 1 *For the BDF3-CS$_{DF}$ and BDF3-CS$_{BD}$ methods, the preconditioners P_{DF} and P_{BD} are the following,*

$$P_{DF} = \frac{11}{6}I - \tau \Delta_N \left(\left(1 - \varepsilon + 3 \overline{\left(u_N^{n,m}\right)^2} \right) I + \Delta_N^2 \right),$$

$$P_{BD} = \frac{11}{6}I - \tau \Delta_N \left(\left(1 + 3 \overline{\left(u_N^{n,m}\right)^2} \right) I + \Delta_N^2 \right).$$

Remark 2 *Note that the BDF3-CS$_{BF}$ method is a three-step scheme and needs u_N^1 and u_N^2 to get started. In our approach in order to have third-order temporal accuracy, we utilize the two-step implicit Runge–Kutta (IMRK) method, which is fourth-order accurate, to compute u_N^1 and u_N^2.*

Remark 3 *Combining the Fourier pseudo-spectral method with the semi-discrete schemes (21)–(22), (36)–(37), and (39)–(40), we can derive the corresponding nonlinear fully discrete BDF3 schemes, for which the optimal rate convergence can be theoretically justified by a careful convergence analysis with the similar proof techniques as in [33, 37–43]. We provide a more specific description below. First of all, we denote $\mathcal{R}$ as,*

$$\mathcal{R} := H^4(0, T; C^0) \cap H^3(0, T; H^{m+2}) \cap L^\infty(0, T; H^{m+6}).$$

Define $U_N(\cdot, t) := \mathcal{P}_N u_e(\cdot, t)$, the (spatially-continuous) Fourier projection of the exact solution $u_e(\cdot, t)$ onto $\mathcal{B}^K$, the space of trigonometric polynomials of degree at most K. Denote U^n as the point projection values of $U_N(\cdot, t_n)$ at discrete grid points, i.e., $U_{i,j}^n = U_N(x_i, y_j, t_n)$ (the 3D case is similar to that in 2D except for an additional index). Let $e^n = U^n - u^n$ be the error function, where u^n is computed by the nonlinear fully discrete BDF3-CS_{BF} scheme. Given initial data $U_N(\cdot, t_0), U_N(\cdot, t_1), U_N(\cdot, t_2) \in C_{per}^{m+6}(\bar{\Omega})$, assume that the unique solution for the PFC (2)–(5) is of regularity class $\mathcal{R}$. Then, provided τ and $h = h_x = h_y$ are sufficiently small, for $n \in \mathbb{N}$, such that $n\tau \leqslant T$, we have the following estimate for the nonlinear fully discrete BDF3-CS_{BF} scheme,

$$\left\| e^n \right\|_2 + \sqrt{\tau \sum_{l=0}^{n} \left\| \nabla_N e^l \right\|_2^2} \leqslant C(\tau^3 + h^m),$$

where $C > 0$ is independent of τ and h. In addition, for the nonlinear fully discrete BDF3-CS_{DF} and BDF3-CS_{BD} schemes, similarly, we can also obtain the optimal rate convergence, $\mathcal{O}(\tau^3 + h^m)$, in the $L_N^\infty(0, T; L_N^2) \cap L_N^2(0, T; H_N^1)$ norm. Note that the norm L_N^∞, L_N^2, and H_N^1 here are the same as in [33].

5 Numerical simulations

In this section, we present several numerical examples of the PFC equation with periodic boundary conditions to verify the accuracy and efficiency of the proposed schemes. In the following numerical simulations, the tolerance tol of the nonlinear iterative solver and of the iterative method for the linear system are both set to be $tol = 10^{-12}$.

5.1 Temporal accuracy test

We perform two numerical simulations to test the convergence rates of the three proposed schemes, the BDF3-CS$_{BF}$, BDF3-CS$_{DF}$, and BDF3-CS$_{BD}$ schemes. These examples are chosen from similar examples in [20, 23–26].

Example 1 We take $\varepsilon = 0.025$ and choose the suitable forcing term to satisfy the following exact solution

$$u(x, y, t) = \sin(\pi x/32) \cos(\pi y/32) \cos t.$$

The computational domain is set to be $\Omega = [0, 128]^2$ and the initial condition is $u_0(x, y) = u(x, y, 0)$. We use 256^2 Fourier modes so that the errors from the spatial discretization are negligible compared with that from the time discretization errors.

In Tables 1 and 2, we list the L^∞ and L^2 errors between the numerical solutions and exact solutions at final time $T = 20$ with different time step sizes τ.

From Tables 1 and 2, we clearly see that the BDF3-CS$_{BF}$, BDF3-CS$_{DF}$, and BDF3-CS$_{BD}$ schemes are all third-order accurate in time.

In this example, we know the exact solution. In the following examples, the exact solutions are not known. We compare the solutions at coarse meshes again that from the finest mesh.

Table 1 The L^∞ errors and temporal convergence rates of Example 1

τ	BDF3-CS$_{BF}$		BDF3-CS$_{DF}$		BDF3-CS$_{BD}$	
	Error	Order	Error	Order	Error	Order
1.0000	1.0997E−01	-	1.0995E−01	-	1.0986E−01	-
0.5000	1.0517E−02	3.3864	1.0533E−02	3.3839	1.0565E−02	3.3783
0.1000	2.0379E−04	2.4503	2.0381E−04	2.4512	2.0386E−04	2.4529
0.0500	2.6840E−05	2.9246	2.6841E−05	2.9247	2.6842E−05	2.9250
0.0100	2.2276E−07	2.9772	2.2275E−07	2.9772	2.2274E−07	2.9773
0.0050	2.7965E−08	2.9938	2.7964E−08	2.9938	2.7962E−08	2.9938
0.0010	2.2480E−10	2.9970	2.2471E−10	2.9972	2.2470E−10	2.9972

Table 2 The L^2 errors and temporal convergence rates of Example 1

τ	BDF3-CS$_{BF}$		BDF3-CS$_{DF}$		BDF3-CS$_{BD}$	
	Error	Order	Error	Order	Error	Order
1.0000	1.0053E+01	-	1.0049E+01	-	1.0042E+01	-
0.5000	4.4119E−01	4.5100	4.4218E−01	4.5062	4.4373E−01	4.5002
0.1000	1.2584E−02	2.2101	1.2584E−02	2.2115	1.2584E−02	2.2137
0.0500	1.6956E−03	2.8917	1.6954E−03	2.8919	1.6952E−03	2.8921
0.0100	1.4308E−05	2.9669	1.4306E−05	2.9669	1.4302E−05	2.9670
0.0050	1.7998E−06	2.9909	1.7995E−06	2.9909	1.7989E−06	2.9910
0.0010	1.4490E−08	2.9961	1.4482E−08	2.9963	1.4478E−08	2.9963

Example 2 In this example, once again, we set $\varepsilon = 0.025$ and $\Omega = [0, 128]^2$. The initial condition is given as

$$u_0(x, y) = \sin(\pi x/32) \cos(\pi y/32).$$

In order to compute the errors, we take the approximate solution calculated by employing BDF3-CS$_{BF}$ (or BDF3-CS$_{DF}$, BDF3-CS$_{BD}$) scheme with the time step $\tau = 0.001$ as the benchmark solution. Besides, we use 256^2 Fourier modes for the spatial discretization.

Figure 2 shows the L^2 errors at $T = 20$ for the phase field variable u with different time step size of $\tau = 1, 0.5, 0.1, 0.05, 0.01, 0.005$, and the L^2 errors at $T = 100$ for the phase field variable u with different time step size of $\tau = 20, 10, 5, 2, 1, 0.1, 0.01$. From Fig. 2, we observe that all the three new developed schemes are third-order accurate in time. In addition, we observe that the L^2 errors at $T = 100$ obtained by using the BDF3-CS$_{BF}$ scheme is smaller than that obtained by using the other two schemes, especially for the larger time step size.

In Fig. 3, we plot the time evolution of the original energy and the modified energy for the PFC equation using the BDF3-CS$_{BF}$ scheme with different temporal resolu-
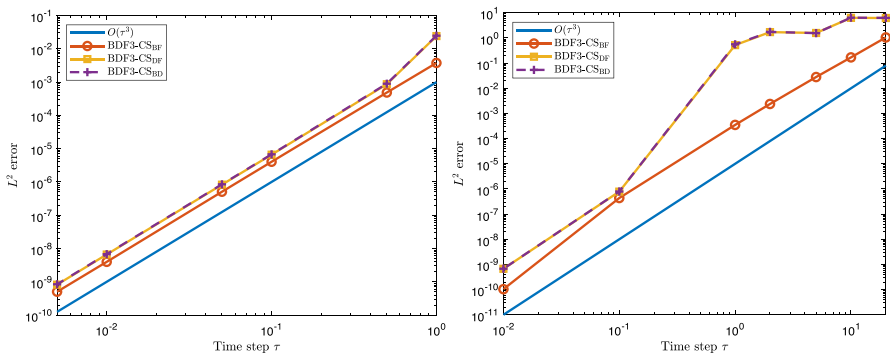
Fig. 2 The L^2 errors at $T = 20$ (Left), 100 (Right) for the phase field variable u with different temporal resolutions of Example 2
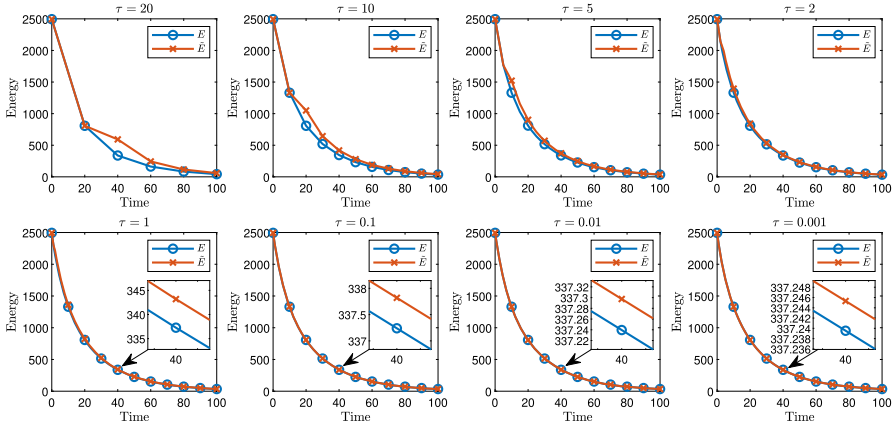
Fig. 3 Time evolution of the original energy E and modified energy $\tilde{E}$ using BDF3-CS$_{BF}$ with different time step of Example 2

tions. It is observed that the modified energy curve is very close to the original energy curve with a small time step size of $\tau = 0.1, 0.01, 0.001$. The energy curves corresponding to the BDF3-CS$_{DF}$ and the BDF3-CS$_{BD}$ schemes are similar to that from the BDF3-CS$_{BF}$ and thus are not shown here.

In Figs. 4, 5, and 6, we plot the time evolution of modified energy functional, and the variations of mass at different times compared to the initial mass. It is observed that the modified energy obtained by using all three schemes is non-increasing at all times, and it means that the numerical result is energy stable. For all the three schemes, the modified energy curves under the time step size of $\tau = 0.1, 0.01, 0.001$ are very close. However, the modified energy curves obtained by using a large time step as $\tau = 5, 10, 20$, is considerably away from the modified energy curves corresponding to the benchmark solution. Besides, we can observe that with different time steps, the variations of mass obtained by using the three schemes are all very small, which indicates that our schemes are mass conserving.
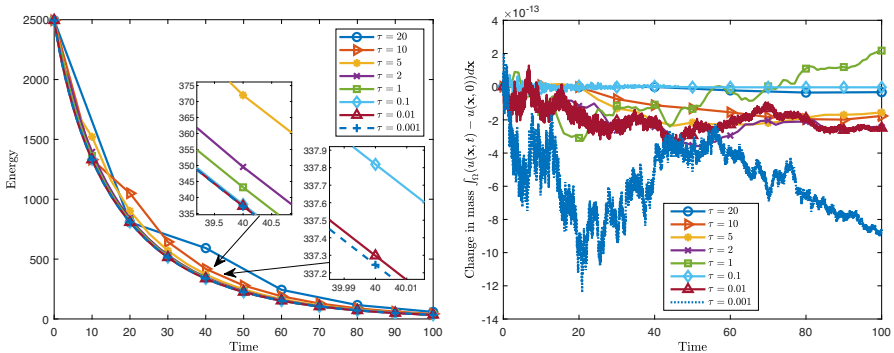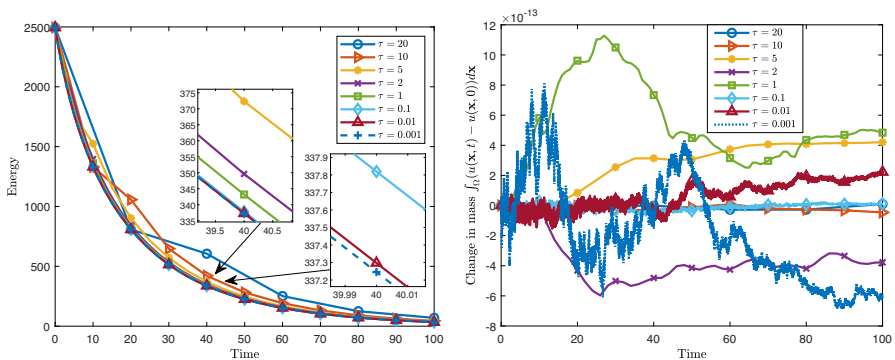

Fig. 4 Time evolution of the modified energy (Left) and the variations of mass at different times compared to the initial mass (Right) of Example 2, calculated by the BDF3-CS$_{BF}$ scheme
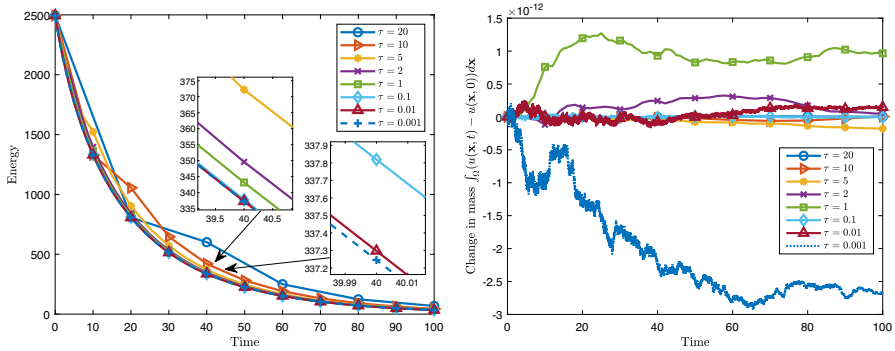
Fig. 5 Time evolution of the modified energy (Left) and the variations of mass at different times compared to the initial mass (Right) of Example 2, calculated by the BDF3-CS$_{DF}$ scheme

5.2 Comparisons of a new scheme with the convex splitting Runge–Kutta method

In this subsection, we present a numerical example of the PFC equation to show the efficiency of the proposed schemes, compared with the third-order convex splitting Runge–Kutta method (CSRK) proposed in [32]. It is worth noting that there are three third-order CSRK schemes presented in [32], which are six stages of diagonal implicit Runge–Kutta methods with different coefficient matrices and have similar computational efficiency. Therefore, in the following numerical example, we only use the BDF3-CS$_{BF}$ scheme proposed in this paper and one of CSRK methods which is denoted as CSRK-$\mathbf{R}_3(1/2)$ from [32] to solve PFC equation for the comparison of efficiency. The example below is chosen from a similar example in [32]. All numerical tests are run on a PC equipped with an intel i7 CPU (Intel Core i7-11800 H Processor), compiled with MATLAB.

Fig. 6 Time evolution of the modified energy (Left) and the variations of mass at different times compared to the initial mass (Right) of Example 2, calculated by the BDF3-CS$_{BD}$ scheme

Example 3 In this example, we set $\varepsilon = 0.2$ and $\Omega = [0, 32]^2$. The initial condition is given by

$$u_0(x, y) = 0.03 + 0.005 \sum_{l=0}^{6} \sum_{m=0}^{6} \text{Re} \left[a_{lm} e^{il\pi x/16} \right] \cdot \text{Re} \left[b_{lm} e^{im\pi y/16} \right],$$

where a_{lm} and b_{lm} are random complex numbers with $|a_{lm}| \leqslant 1$ and $|b_{lm}| \leqslant 1$. We use the computed solution from the BDF3-CS$_{\text{BF}}$ scheme with a small time step size $\tau = 0.001$ as the benchmark solution. We use 64^2 Fourier modes for the spatial discretization.

In Table 3, we list the L^2 errors at the final time $T = 128$ with different time step sizes of $\tau = 2, 1, 0.5, 0.25, 0.125, 0.0625$. In addition, the number of nonlinear iterations averaged over the simulation time $0 \leqslant n\tau \leqslant T$ and the CPU time in seconds are shown in Table 3. After simple calculations based on the data of Table 3, we know that the error using BDF3-CS$_{\text{BF}}$ scheme is almost twice that of the CSRK-$\mathbf{R}_3(1/2)$ method and both the two schemes have third-order accuracy. However, the running time and number of nonlinear iterations for BDF3-CS$_{\text{BF}}$ scheme is just about one-sixth that of CSRK-$\mathbf{R}_3(1/2)$ method. Therefore, from Table 3, we clearly see that the BDF3-CS$_{\text{BF}}$ is more efficient than CSRK-$\mathbf{R}_3(1/2)$.

5.3 Crystal growth in a supercooled liquid

In this subsection, we give two simulations of the crystal growth in a supercooled liquid in the case of two and three-dimensional space, using the BDF3-CS$_{\text{BF}}$ scheme. These examples are chosen from similar examples in [11, 15, 19, 24, 26, 27].

Example 4 In this example, we set the computational domain as $[0, 800]^2$ and define the 2D crystallites initially as

$$u_0(x_l, y_l) = \bar{u} + C \left(\cos \left(q y_l / \sqrt{3} \right) \cos (q x_l) - 0.5 \cos \left(2 q y_l / \sqrt{3} \right) \right), \quad l = 1, 2, 3,$$

where x_l and y_l define a local system of cartesian coordinates that is oriented with the crystallite lattice. In order to obtain crystallites with different orientations, we

Table 3 Comparision of BDF3-CS$_{\text{BF}}$ scheme and CSRK-$\mathbf{R}_3(1/2)$ method of Example 3

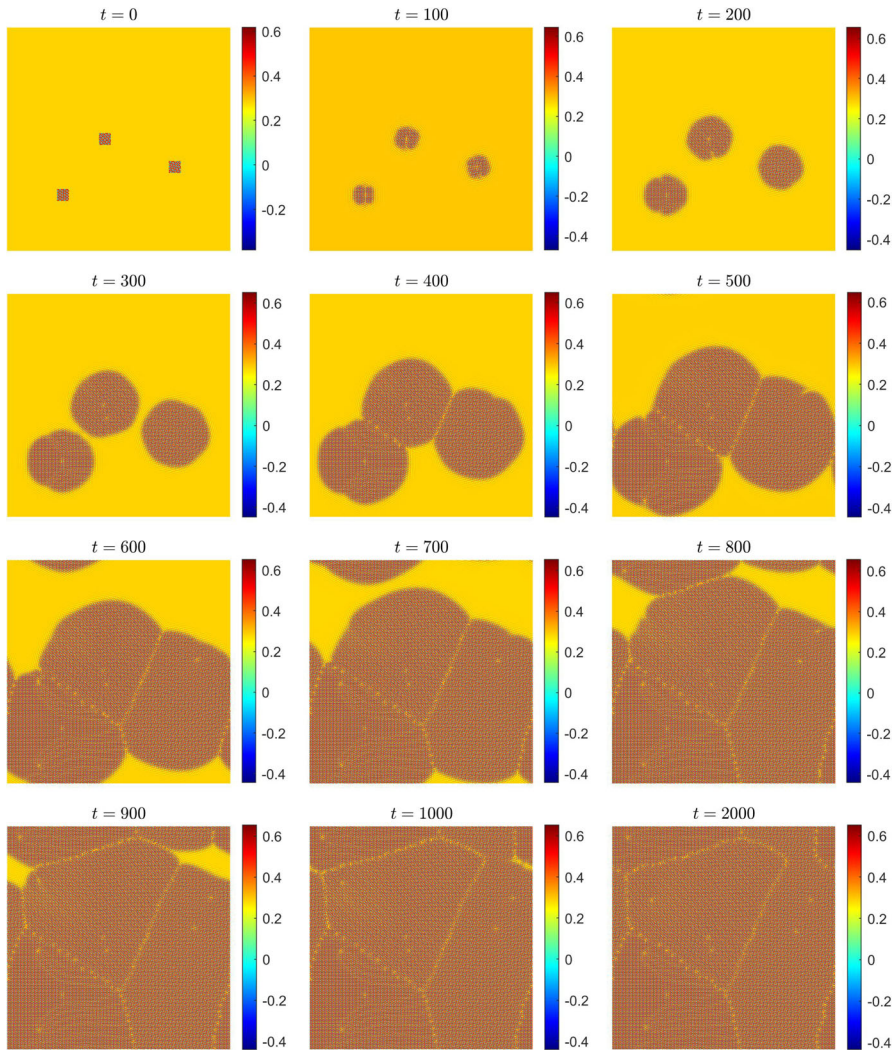| τ	BDF3-CS$_{\text{BF}}$				CSRK-$\mathbf{R}_3(1/2)$			
	Error	Order	Iterations	Time	Error	Order	Iterations	Time
2.0000	1.69E−01	-	4.13	1.19	1.19E−01	-	28.00	6.65
1.0000	3.55E−02	2.25	3.92	1.87	1.86E−02	2.68	22.79	10.92
0.5000	5.65E−03	2.65	3.63	3.10	2.54E−03	2.87	20.28	16.63
0.2500	7.93E−04	2.83	3.16	4.72	3.29E−04	2.95	18.63	27.99
0.1250	1.05E−04	2.92	3.00	8.22	4.17E−05	2.98	18.00	50.29
0.0625	1.35E−05	2.96	3.00	16.24	5.24E−06	2.99	18.00	96.47

Fig. 7 Evolution of the crystal growth in a supercooled liquid of Example 4

first use the affine transformation of the global coordinates (x, y) to define the local coordinates (x_l, y_l) with a rotation given by an angle θ, that is,

$$x_l(x, y) = x \sin(\theta) + y \cos(\theta),$$
$$y_l(x, y) = -x \cos(\theta) + y \sin(\theta).$$

The constant parameters above are take as $\bar{u} = 0.285$, $C = 0.446$, and $q = 0.66$ and the rotation angles θ are chosen as $\theta = -\pi/4, 0, \pi/4$. We then set three perfect crystallites in three small square patches of the computational domain. The centers of
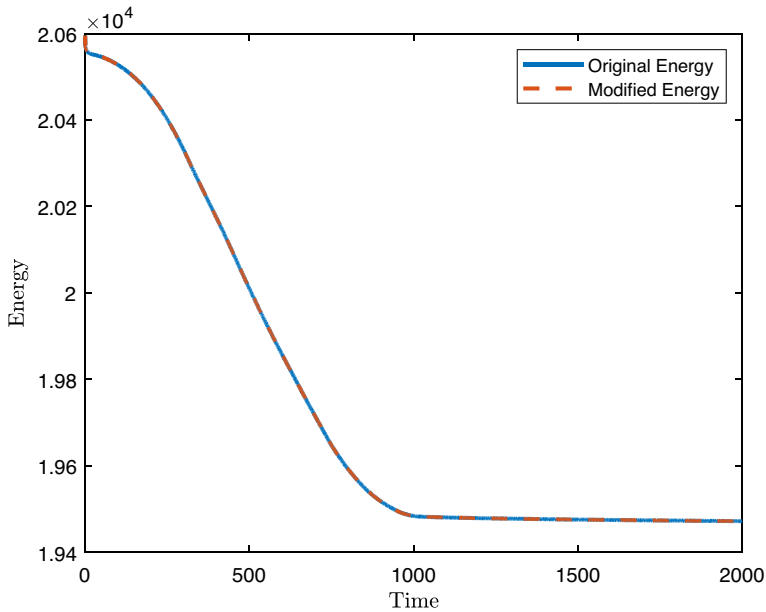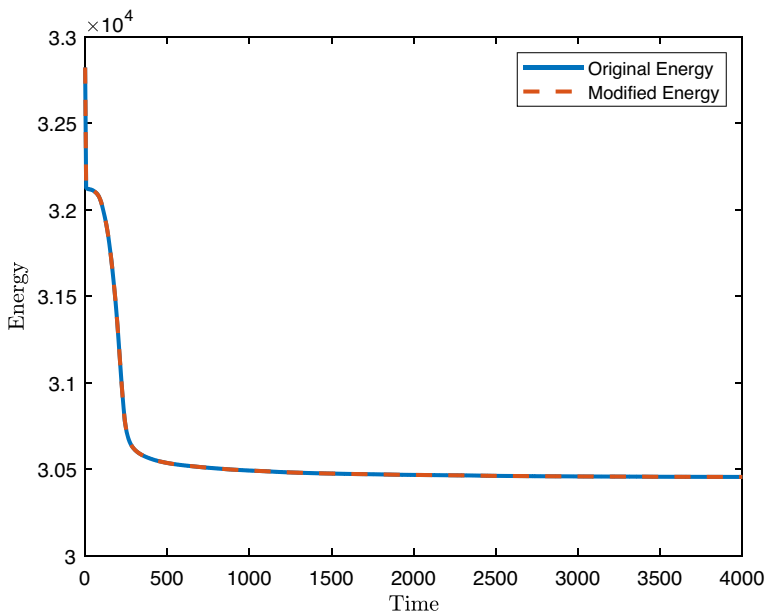
Fig. 8 Time evolution of the original and modified energy for the crystal growth in a supercooled liquid of Example 4

the three square are located at (200, 200), (350, 400), and (600, 300). And the length of each patch is 40.

We use 512^2 Fourier modes for the discretization of two-dimensional space and choose the relatively small step in time, i.e., $\tau = 0.1$. Besides, we set the parameter $\varepsilon = 0.25$ and final time $T = 2000$.

In Fig. 7, we present the snapshots of the numerical solution at $t = 0, 100, 200, 300, 400, 500, 600, 700, 800, 900, 1000, 2000$. We can observe that the growth of the crystalline phase and the evolution of crystal-liquid interfaces. In addition, it can be clearly observed that the different alignment of the crystallites causes defects and dislocations.

Moreover, the evolution of the original and modified energy are shown in Fig. 8. It is clearly displayed that the energy monotonically decays all the time. In other word, the result of the numerical simulation in this example is energy stable.

Example 5 We present the simulation for the growth and interaction of two crystallites inside the computational domain $[0, 100]^3$. The 3D initial crystallites are initially defined as

$$u_0(x_l, y_l, z_l) = \bar{u} + C\left(\cos(ax_l)\cos(by_l) + \cos(ax_l)\cos(cz_l)\right.$$
$$\left. + \cos(by_l)\cos(cz_l) - 0.5\cos(by_l)\right),$$
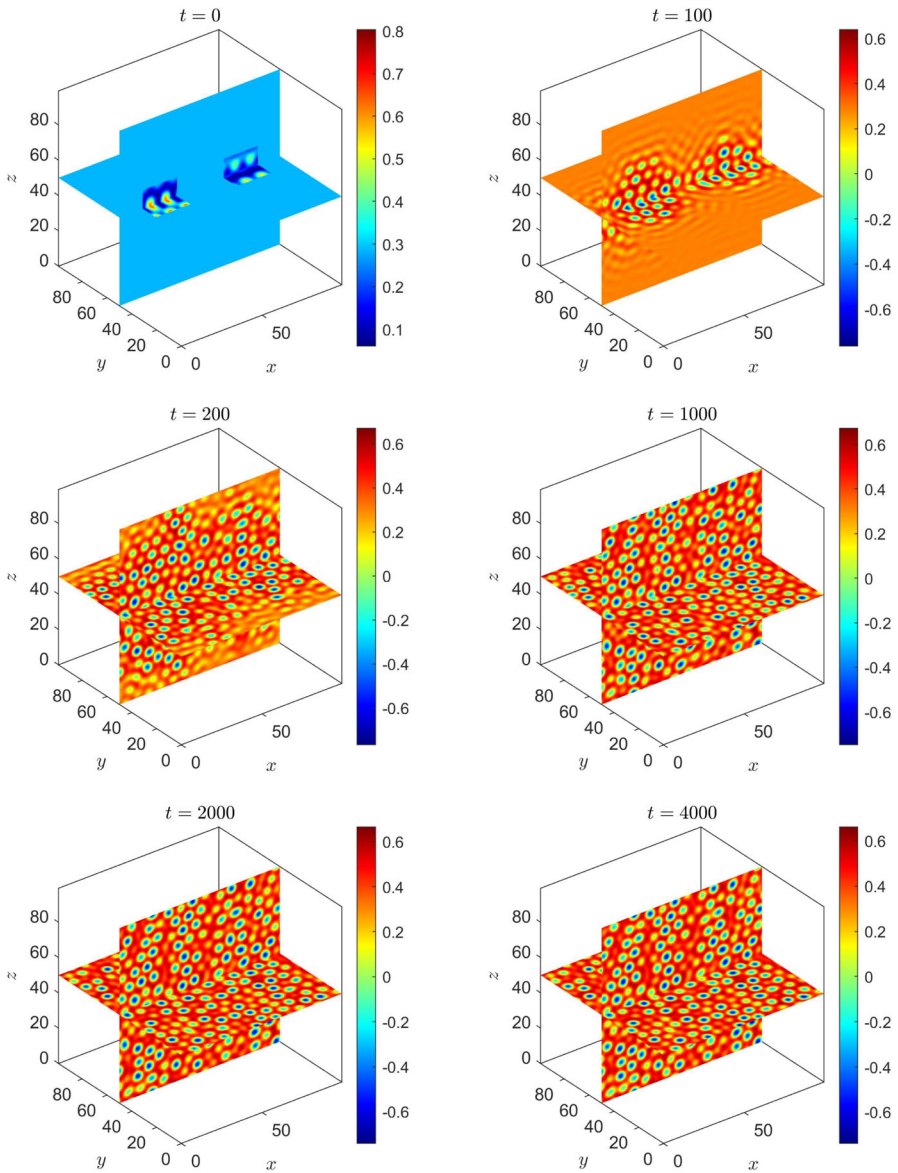
Fig. 9 The snapshots of the numerical approximation at $t = 0, 100, 200, 1000, 2000, 4000$ of Example 5

where x_l, y_l, and z_l define a local system of Cartesian coordinates which is oriented with the crystallite lattice. The local Cartesian system (x_l, y_l, z_l) is defined as

$$x_l(x, y, z) = x,$$
$$y_l(x, y, z) = y \cos \theta - z \sin \theta,$$
$$z_l(x, y, z) = y \sin \theta + z \cos \theta.$$
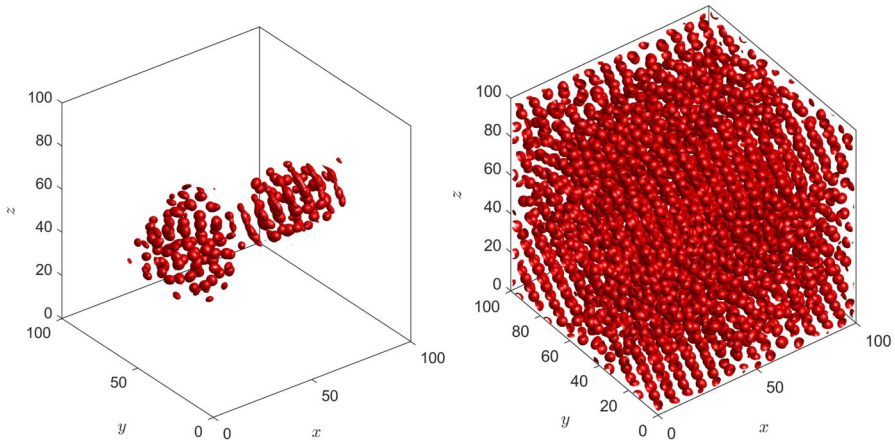
Fig. 10 The isosurface of $u = 0$ at $t = 100$ (Left), 4000 (Right) of Example 5

The centers of the two small cube blocks are located at (25, 50, 50) and (75, 50, 50), and the length of each cube is 20. The parameters above are take as $\bar{u} = 0.285$, $C = 0.15$, $a = 0.66$, $b = 0.38$, $c = 0.46$, and the rotation angle θ are chosen as $\theta = \pi/6, -\pi/6$. The other parameters are $\varepsilon = 0.25$ and $T = 4000$. We use 128^3 Fourier modes to discretize the three-dimensional space and choose the relatively small time step i.e. $\tau = 0.1$.

Fig. 11 Time evolution of the original and modified energy for the crystal growth in a supercooled liquid of Example 5
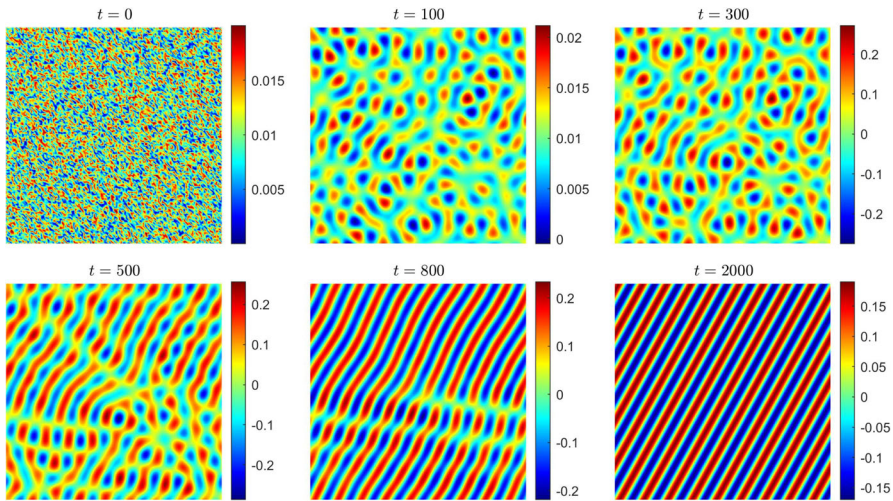
Fig. 12 The evolution of the phase transition behavior in two-dimensional space with $\bar{u} = 0.01$ of Example 6. Snapshots of the numerical approximation of density field u are taken at $t = 0, 100, 300, 500, 800, 2000$

In Fig. 9, we show the snapshots of the numerical solution at $t = 0, 100, 200, 1000, 2000, 4000$. In Fig. 10, we display the isosurface of the numerical solution at $t = 100, 4000$. From Figs. 9 and 10, we can observe that the growth of the crystalline phase and the evolution of crystal-liquid interfaces are effected by different alignments of crystallites.
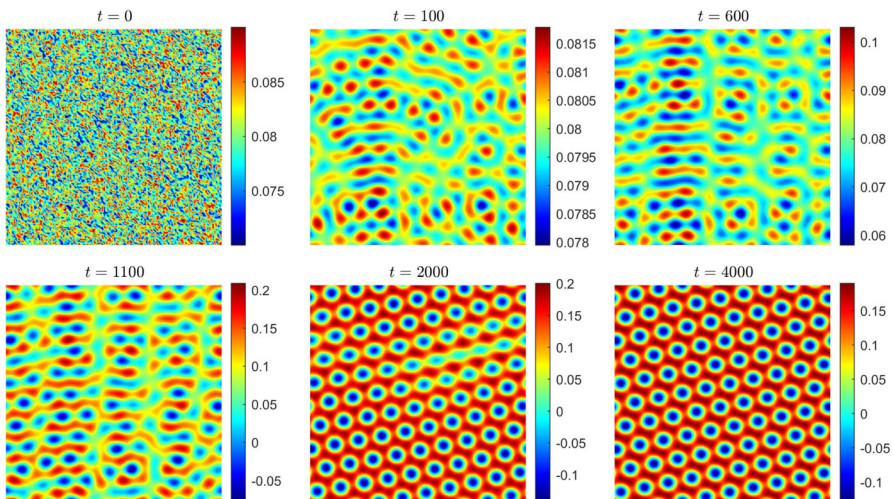
Fig. 13 The evolution of the phase transition behavior in 2D with $\bar{u} = 0.08$ of Example 6. The snapshots of the numerical approximation of density field u are taken at $t = 0, 100, 600, 1100, 2000, 4000$
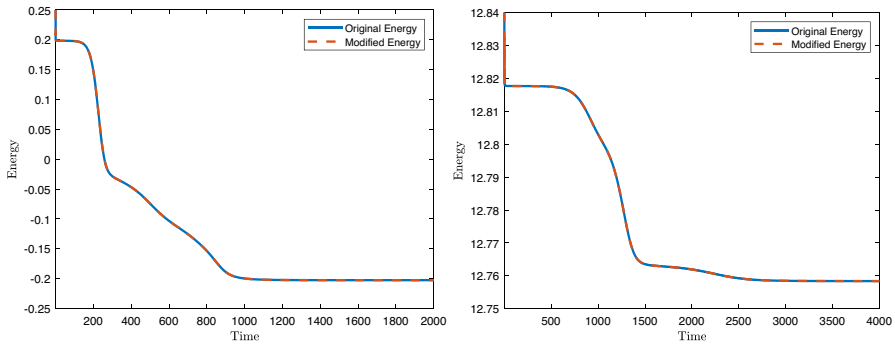
Fig. 14 The evolution of the original and modify energy for phase transition behavior in two-dimensional space with $\bar{u} = 0.01$ (Left) and $\bar{u} = 0.08$ (Right) of Example 6

Besides, the evolution of the original and modified energy are displayed in Fig. 11. It is clearly shown that both the original energy and modified energy are non-increasing. That is, the numerical result here is energy stable.

5.4 Phase transition behaviors

In this subsection, we present the simulations of the phase transition behavior in two and three dimensions with two examples. The BDF3-CS$_{\text{BF}}$ scheme is used to simulate the evolution here. These examples are chosen from similar examples in [15, 20, 23, 24, 26–28].

Example 6 With the computational domain of $[0, 64]^2$ and the random initial data $u_{ij} = \bar{u} + \eta_{ij}$, where η_{ij} is uniformly distributed random number satisfying $\left|\eta_{ij}\right| \leqslant 0.01$ at the grid points, we use 128^2 Fourier modes to discretize the two-dimensional space and choose the time step size as $\tau = 0.1$ for better accuracy. The other parameter is $\varepsilon = 0.025$.

In Figs. 12 and 13, we present the evolution of the phase transition behavior with $\bar{u} = 0.01$ and $\bar{u} = 0.08$, respectively. We obtain the patterns of stripes in Fig. 12 and attain the patterns of triangles in Fig. 13.

In Fig. 14, we show the evolution of the original and modified energy for phase transition with $\bar{u} = 0.01$ and $\bar{u} = 0.8$. It can be clearly observed that both the original energy and modified energy are decreasing at all times, which also provides numerical evidence for the energy stability of the proposed schemes.

Example 7 For the three-dimensional case, with the computational domain of $[0, 64]^3$ and the random initial data $u_{ijk} = \bar{u} + \eta_{ijk}$, where $\bar{u} = 0.08$ and η_{ijk} is uniformly distributed random number satisfying $\left|\eta_{ijk}\right| \leqslant 0.01$ at the grid points, we use 128^3 Fourier modes for the discretization of the three-dimensional space. The time step is $\tau = 0.1$ and the other parameter is $\varepsilon = 0.025$.
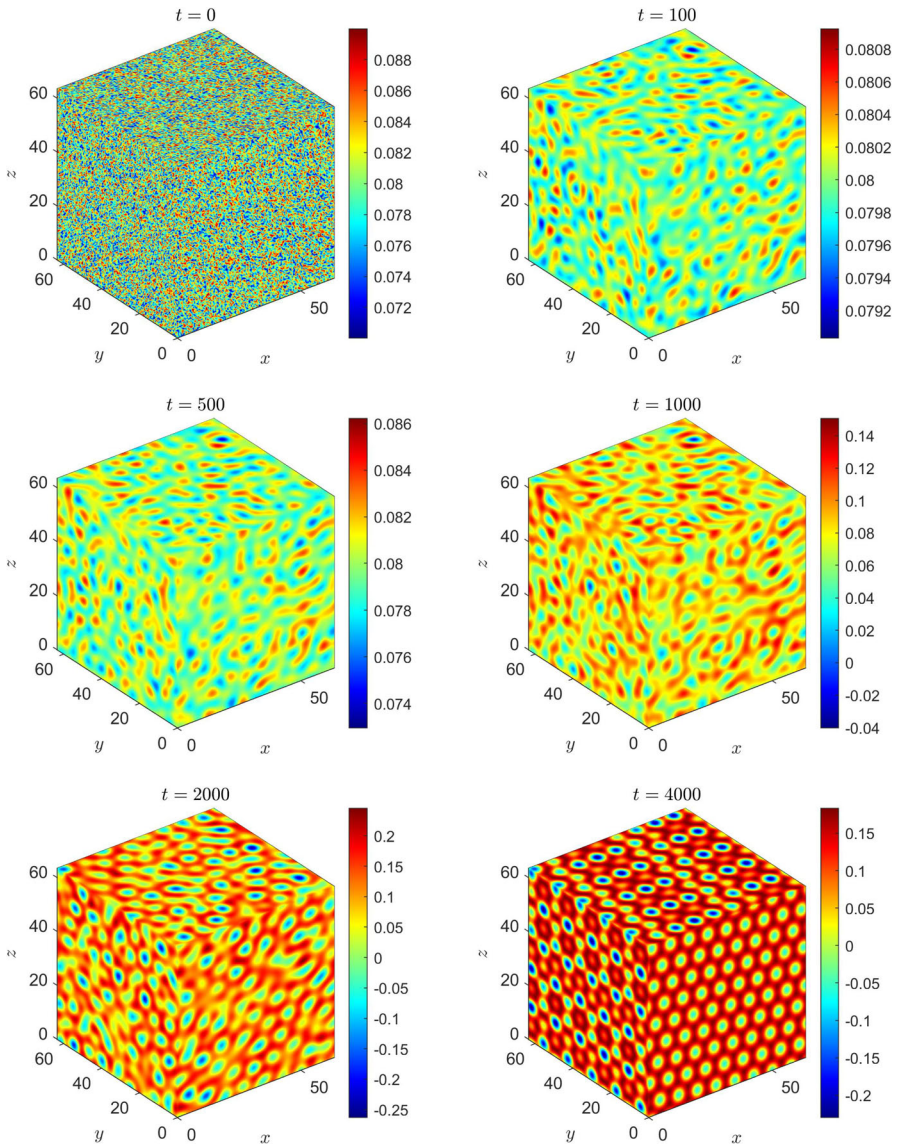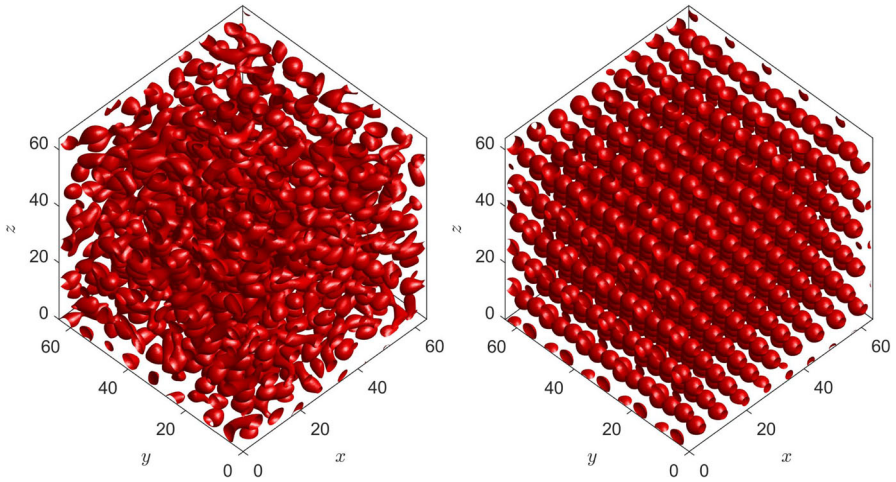
Fig. 15 The evolution of the 3D phase transition behavior of Example 7. The snapshots of the numerical approximation of density field u are taken at $t = 0, 100, 500, 1000, 2000, 4000$

In Figs. 15 and 16, we present the evolution of the phase transition behavior at different times. In Fig. 17, we show the evolution of the original and modify energy. It can be observed that the two types of energy are decreasing at all times, which provides numerical evidence for the energy stability of the proposed schemes again.

Fig. 16 The evolution of the 3D phase transition behavior of Example 7. Iso-surface of $u = 0$ are taken at $t = 2000$ (Left), 4000 (Right)

6 Concluding remarks

In this paper, based on the three types of convex splitting of Swift-Hohenberg energy functional and using the BDF3 formula for temporal discretization, we proposed three
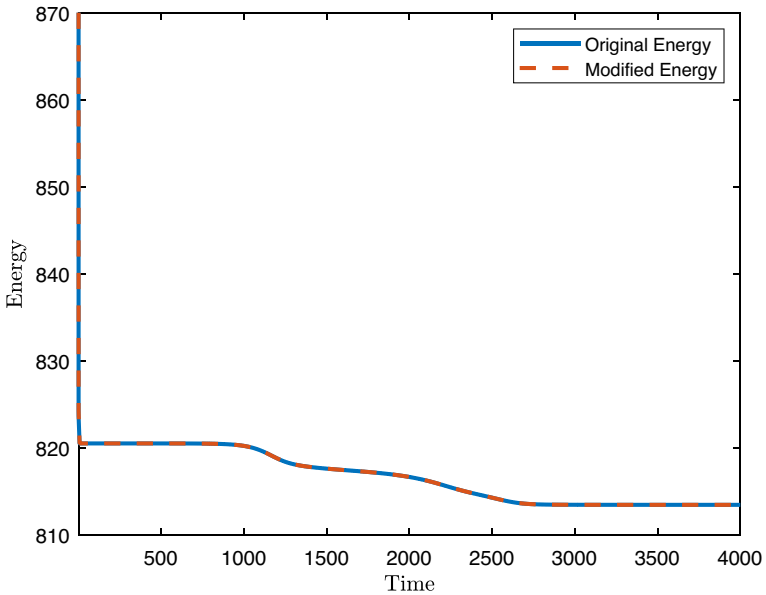
Fig. 17 The evolution of the original and modify energy for phase transition behavior in three dimensional of Example 7

third-order accurate (in time) numerical schemes to solve the PFC equation with periodic boundary conditions. Furthermore, we rigorously proved that the proposed schemes are mass conserving and uniquely solvable with any time steps. We presented rigorous proofs of the energy stability under the assumption of the time step satisfying given conditions. We also analyzed the similarities and differences between the three methods and found out that the BDF3-CS$_{\text{BF}}$ scheme has a more relaxed time step size constraint. Furthermore, combined with the Fourier pseudo-spectral method in the spatial discretization, the fully discrete schemes and their implementation based on nonlinear iterative methods were presented. Various two and three-dimensional numerical experiments were performed to validate the accuracy, energy stability, mass conservation, and efficiency of the schemes proposed in this paper. The numerical simulations indicated that the BDF3-CS$_{\text{BF}}$, BDF3-CS$_{\text{DF}}$, and BDF3-CS$_{\text{BD}}$ schemes are all third-order accurate in time, and the BDF3-CSBF scheme often has better accuracy compared to the other two. Simulations of long-term behaviors of the PFC equation against the problems with the exact solution and the benchmark problems in the literature showed that all three new developed methods are reasonable choices for solving the PFC equation among which the BDF3-CS$_{\text{BF}}$ scheme is more favorable to the other two schemes.

Appendix A. Proofs of theorems in Subsection 3.2

We skip the proofs of Theorems 4, 5, 7, and 8 since it is very similar to Theorems 1 and 2. In what follows, we give the proofs of Theorems 6 and 9.

A.1 Proof of Theorem 6

Proof Combining the (36) and (37), we obtain

$$
\frac{\frac{11}{6}u^{n+1} - 3u^n + \frac{3}{2}u^{n-1} - \frac{1}{3}u^{n-2}}{\tau} - (1-\varepsilon)\Delta u^{n+1} - \Delta^3 u^{n+1}
$$
$$
-\Delta\left(u^{n+1}\right)^3 - 2\Delta^2\left(3u^n - 3u^{n-1} + u^{n-2}\right) = 0. \qquad (A.1)
$$

Taking the inner product of (A.1) with $(-\Delta)^{-1}\left(u^{n+1} - u^n\right)$, we have

$$
0 = \left(\frac{\frac{11}{6}u^{n+1} - 3u^n + \frac{3}{2}u^{n-1} - \frac{1}{3}u^{n-2}}{\tau}, (-\Delta)^{-1}\left(u^{n+1} - u^n\right)\right)
$$
$$
+ \left(-(1-\varepsilon)\Delta u^{n+1}, (-\Delta)^{-1}\left(u^{n+1} - u^n\right)\right)
$$
$$
+ \left(-\Delta^3 u^{n+1}, (-\Delta)^{-1}\left(u^{n+1} - u^n\right)\right)
$$

$$+ \left(-\Delta \left(u^{n+1} \right)^3, (-\Delta)^{-1} \left(u^{n+1} - u^n \right) \right)$$
$$+ \left(-2\Delta^2 \left(3u^n - 3u^{n-1} + u^{n-2} \right), (-\Delta)^{-1} \left(u^{n+1} - u^n \right) \right). \tag{A.2}$$

From the second term of (A.2), we further derive

$$\left(-(1-\varepsilon)\Delta u^{n+1}, (-\Delta)^{-1} \left(u^{n+1} - u^n \right) \right)$$
$$= (1-\varepsilon) \left(u^{n+1}, u^{n+1} - u^n \right)$$
$$= \frac{1-\varepsilon}{2} \left(\left\| u^{n+1} \right\|^2 - \left\| u^n \right\|^2 + \left\| u^{n+1} - u^n \right\|^2 \right). \tag{A.3}$$

From the third term of (A.2), we know that

$$\left(-\Delta^3 u^{n+1}, (-\Delta)^{-1} \left(u^{n+1} - u^n \right) \right)$$
$$= \left(\Delta u^{n+1}, \Delta \left(u^{n+1} - u^n \right) \right)$$
$$= \frac{1}{2} \left\| \Delta u^{n+1} \right\|^2 - \frac{1}{2} \left\| \Delta u^n \right\|^2 + \frac{1}{2} \left\| \Delta \left(u^{n+1} - u^n \right) \right\|^2. \tag{A.4}$$

Next, from the fifth term of (A.2), similar to (32), we continue to derive

$$\left(-2\Delta^2 \left(3u^n - 3u^{n-1} + u^{n-2} \right), (-\Delta)^{-1} \left(u^{n+1} - u^n \right) \right)$$
$$= -2 \left(\nabla \left(3u^n - 3u^{n-1} + u^{n-2} \right), \nabla \left(u^{n+1} - u^n \right) \right)$$
$$\geqslant - \left(\left\| \nabla u^{n+1} \right\|^2 - \left\| \nabla u^n \right\|^2 \right) + \left(\left\| \nabla \left(u^{n+1} - u^n \right) \right\|^2 - \left\| \nabla \left(u^n - u^{n-1} \right) \right\|^2 \right)$$
$$+ \left(\left\| \nabla \left(u^{n+1} - 2u^n + u^{n-1} \right) \right\|^2 - \left\| \nabla \left(u^n - 2u^{n-1} + u^{n-2} \right) \right\|^2 \right)$$
$$- 2 \left\| \nabla \left(u^{n+1} - u^n \right) \right\|^2. \tag{A.5}$$

In addition, the first term of (A.2) is the same as (29), and the fourth term of (A.2) is the same as (31).

In summary, combining (29), (31), (38), (A.2)–(A.5), we obtain

$$\tilde{E}_{DF}^{n+1} - \tilde{E}_{DF}^n + \frac{5}{6\tau} \left\| u^{n+1} - u^n \right\|_{-1}^2 + \frac{1-\varepsilon}{2} \left\| u^{n+1} - u^n \right\|^2$$
$$+ \frac{1}{2} \left\| \Delta \left(u^{n+1} - u^n \right) \right\|^2 - 2 \left\| \nabla \left(u^{n+1} - u^n \right) \right\|^2 \leqslant 0. \tag{A.6}$$

According to Lemma 1, we have

$$\frac{5}{6\tau}\left\|u^{n+1}-u^n\right\|_{-1}^2 + \frac{1-\varepsilon}{2}\left\|u^{n+1}-u^n\right\|^2 + \frac{1}{2}\left\|\Delta\left(u^{n+1}-u^n\right)\right\|^2$$
$$\geqslant \left(\sqrt{2\sqrt{\frac{10\lambda}{3\tau}}+1}-\varepsilon-\lambda\right)\left\|\nabla\left(u^{n+1}-u^n\right)\right\|^2, \tag{A.7}$$

where $\lambda \in \mathbb{R}$ such that $\lambda > 0$, and $2\sqrt{\frac{10\lambda}{3\tau}}+1-\varepsilon \geqslant 0$. Substitute (A.7) into (A.6), we obtain

$$\tilde{E}_{DF}^{n+1} - \tilde{E}_{DF}^n + \left(\sqrt{2\sqrt{\frac{10\lambda}{3\tau}}+1}-\varepsilon-2-\lambda\right)\left\|\nabla\left(u^{n+1}-u^n\right)\right\|^2 \leqslant 0.$$

Obviously, we have $\tilde{E}_{DF}^{n+1} \leqslant \tilde{E}_{DF}^n$, if the following inequality holds,

$$\sqrt{2\sqrt{\frac{10\lambda}{3\tau}}+1}-\varepsilon-2-\lambda \geqslant 0,$$

which is equivalent to

$$\tau \leqslant \frac{40\lambda}{3\left(\lambda^2+4\lambda+3+\varepsilon\right)^2}.$$

We define a function $f_{DF}(\lambda,\varepsilon) = \frac{40\lambda}{3(\lambda^2+4\lambda+3+\varepsilon)^2}$. For any given value of ε satisfying $0 < \varepsilon < 1$, if $\tau \leqslant \max_\lambda f_{DF}(\lambda,\varepsilon)$, then we can derive $\tilde{E}_{DF}^{n+1} \leqslant \tilde{E}_{DF}^n$. We can see that $\max_\lambda f_{DF}(\lambda,\varepsilon) = f_{DF}(\lambda_{DF}^*,\varepsilon)$ for a fixed value of ε, where $\lambda_{DF}^* = \frac{\sqrt{13+3\varepsilon}-2}{3}$. Note that $f_{DF}(\lambda_{DF}^*,\varepsilon) = \frac{45(\sqrt{13+3\varepsilon}-2)}{2(3\varepsilon+5+2\sqrt{13+3\varepsilon})^2} = S_{DF}(\varepsilon)$.

Thus, if the time step τ satisfying $\tau \leqslant S_{DF}(\varepsilon)$, we conclude that $\tilde{E}_{DF}^{n+1} \leqslant \tilde{E}_{DF}^n$, which completes the proof of the theorem.

A.2 Proof of Theorem 9

Proof Combining the (39) and (40), we obtain

$$\frac{\frac{11}{6}u^{n+1}-3u^n+\frac{3}{2}u^{n-1}-\frac{1}{3}u^{n-2}}{\tau} - \Delta u^{n+1} - \Delta^3 u^{n+1} - \Delta\left(u^{n+1}\right)^3$$
$$+\varepsilon\Delta\left(3u^n-3u^{n-1}+u^{n-2}\right) - 2\Delta^2\left(3u^n-3u^{n-1}+u^{n-2}\right) = 0. \tag{A.8}$$

Taking the inner product of (A.8) with $(-\Delta)^{-1}\left(u^{n+1}-u^n\right)$, we have

$$
0 = \left(\frac{\frac{11}{6}u^{n+1}-3u^n+\frac{3}{2}u^{n-1}-\frac{1}{3}u^{n-2}}{\tau}, (-\Delta)^{-1}\left(u^{n+1}-u^n\right)\right)
$$
$$
+\left(-\Delta u^{n+1}, (-\Delta)^{-1}\left(u^{n+1}-u^n\right)\right) + \left(-\Delta^3 u^{n+1}, (-\Delta)^{-1}\left(u^{n+1}-u^n\right)\right)
$$
$$
+\left(-\Delta\left(u^{n+1}\right)^3, (-\Delta)^{-1}\left(u^{n+1}-u^n\right)\right)
$$
$$
+\left(\varepsilon\Delta\left(3u^n-3u^{n-1}+u^{n-2}\right), (-\Delta)^{-1}\left(u^{n+1}-u^n\right)\right)
$$
$$
+\left(-2\Delta^2\left(3u^n-3u^{n-1}+u^{n-2}\right), (-\Delta)^{-1}\left(u^{n+1}-u^n\right)\right). \tag{A.9}
$$

From the seccond term of (A.9), similar to (A.3), we know that

$$
\left(-\Delta u^{n+1}, (-\Delta)^{-1}\left(u^{n+1}-u^n\right)\right) = \frac{1}{2}\left\|u^{n+1}\right\|^2 - \frac{1}{2}\left\|u^n\right\|^2 + \frac{1}{2}\left\|u^{n+1}-u^n\right\|^2. \tag{A.10}
$$

In addition, the first, third, fourth, fifth and sixth term of (A.9) is the same as (29), (A.4), (31), (32), and (A.5), respectively.

Thus, combining (29), (31), (32), (A.4), (A.5), (41), and (A.10), we obtain

$$
\tilde{E}_{BD}^{n+1} - \tilde{E}_{BD}^n + \frac{5}{6\tau}\left\|u^{n+1}-u^n\right\|_{-1}^2 + \frac{1-2\varepsilon}{2}\left\|u^{n+1}-u^n\right\|^2
$$
$$
+\frac{1}{2}\left\|\Delta\left(u^{n+1}-u^n\right)\right\|^2 - 2\left\|\nabla\left(u^{n+1}-u^n\right)\right\|^2 \leqslant 0. \tag{A.11}
$$

According to Lemma 1, we have

$$
\frac{5}{6\tau}\left\|u^{n+1}-u^n\right\|_{-1}^2 + \frac{1-2\varepsilon}{2}\left\|u^{n+1}-u^n\right\|^2 + \frac{1}{2}\left\|\Delta\left(u^{n+1}-u^n\right)\right\|^2
$$
$$
\geqslant \left(\sqrt{2\sqrt{\frac{10\lambda}{3\tau}}+1-2\varepsilon}-\lambda\right)\left\|\nabla\left(u^{n+1}-u^n\right)\right\|^2, \tag{A.12}
$$

where $\lambda \in \mathbb{R}$ such that $\lambda > 0$, and $2\sqrt{\frac{10\lambda}{3\tau}}+1-2\varepsilon \geqslant 0$. Substitute (A.12) into (A.11), we attain

$$
\tilde{E}_{BD}^{n+1} - \tilde{E}_{BD}^n + \left(\sqrt{2\sqrt{\frac{10\lambda}{3\tau}}+1-2\varepsilon}-2-\lambda\right)\left\|\nabla\left(u^{n+1}-u^n\right)\right\|^2 \leqslant 0.
$$

Obviously, we have $\tilde{E}_{BD}^{n+1} \leqslant \tilde{E}_{BD}^n$, if the following inequality holds,

$$\sqrt{2\sqrt{\frac{10\lambda}{3\tau} + 1} - 2\varepsilon - 2} - \lambda \geqslant 0,$$

which is equivalent to

$$\tau \leqslant \frac{40\lambda}{3\left(\lambda^2 + 4\lambda + 3 + 2\varepsilon\right)^2}.$$

We difine a function $f_{BD}\left(\lambda, \varepsilon\right) = \frac{40\lambda}{3\left(\lambda^2+4\lambda+3+2\varepsilon\right)^2}$. For any given value of ε satisfying $0 < \varepsilon < 1$, if $\tau \leqslant \max_\lambda f_{BD}\left(\lambda, \varepsilon\right)$, then we can get $\tilde{E}_{BD}^{n+1} \leqslant \tilde{E}_{BD}^n$. We can see that $\max_\lambda f_{BD}\left(\lambda, \varepsilon\right) = f_{BD}\left(\lambda_{BD}^*, \varepsilon\right)$ for a fixed value of ε, where $\lambda_{BD}^* = \frac{\sqrt{13+6\varepsilon}-2}{3}$. Note that $f_{BD}\left(\lambda_{BD}^*, \varepsilon\right) = \frac{45\left(\sqrt{13+6\varepsilon}-2\right)}{2\left(6\varepsilon+5+2\sqrt{13+6\varepsilon}\right)^2} = S_{BD}(\varepsilon)$.

Thus, if the time step τ satisfying $\tau \leqslant S_{BD}(\varepsilon)$, we conclude that $\tilde{E}_{BD}^{n+1} \leqslant \tilde{E}_{BD}^n$, which completes the proof of the theorem.

Declarations

Conflict of interest The authors declare no competing interests.

References

1. Elder, K.R., Katakowski, M., Haataja, M., Grant, M.: Modeling elasticity in crystal growth. Phys. Rev. Lett. **88**(24), 2457011–2457014 (2002). https://doi.org/10.1103/PhysRevLett.88.245701
2. Elder, K.R., Grant, M.: Modeling elastic and plastic deformations in nonequilibrium processing using phase field crystals. Phys. Rev. E **70**(5), 051605 (2004). https://doi.org/10.1103/PhysRevE.70.051605
3. Elder, K.R., Provatas, N., Berry, J., Stefanovic, P., Grant, M.: Phase-field crystal modeling and classical density functional theory of freezing. Phys. Rev. B **75**(6) (2007). https://doi.org/10.1103/PhysRevB.75.064107
4. Provatas, N., Dantzig, J.A., Athreya, B., Chan, P., Stefanovic, P., Goldenfeld, N., Elder, K.R.: Using the phase-field crystal method in the multi-scale modeling of microstructure evolution. JOM-US **59**(7), 83–90 (2007). https://doi.org/10.1007/s11837-007-0095-3

5. Hirouchi, T., Takaki, T., Tomita, Y.: Development of numerical scheme for phase field crystal deformation simulation. Comp. Mater. Sci. **44**(4), 1192–1197 (2009). https://doi.org/10.1016/j.commatsci.2008.08.001

6. Hirouchi, T., Takaki, T., Tomita, Y.: Effects of temperature and grain size on phase-field-crystal deformation simulation. Int. J. Mech. Sci. **52**(2), 309–319 (2010). https://doi.org/10.1016/j.ijmecsci.2009.09.036

7. Backofen, R., Rätz, A., Voigt, A.: Nucleation and growth by a phase field crystal (PFC) model. Phil. Mag. Lett. **87**(11), 813–820 (2007). https://doi.org/10.1080/09500830701481737

8. Cheng, M., Warren, J.A.: An efficient algorithm for solving the phase field crystal model. J. Comput. Phys. **227**(12), 6241–6248 (2008). https://doi.org/10.1016/j.jcp.2008.03.012

9. Eyre, D.J., Bullard, J.W., Kalia, R., Stoneham, M., Chen, L.-Q.: Unconditionally gradient stable time marching the Cahn-Hilliard equation. Mat. Res. Soc. Symp. Proc. **529** (1998). https://doi.org/10.1557/PROC-529-39

10. Wise, S.M., Wang, C., Lowengrub, J.S.: An energy-stable and convergent finite-difference scheme for the phase field crystal equation. SIAM J. Numer. Anal. **47**(3), 2269–2288 (2009). https://doi.org/10.1137/080738143

11. Hu, Z., Wise, S.M., Wang, C., Lowengrub, J.S.: Stable and efficient finite-difference nonlinear-multigrid schemes for the phase field crystal equation. J. Comput. Phys. **228**(15), 5323–5339 (2009). https://doi.org/10.1016/j.jcp.2009.04.020

12. Elsey, M., Wirth, B.: A simple and efficient scheme for phase field crystal simulation. ESAIM Math. Model. Numer. Anal. **47**(5), 1413–1432 (2013). https://doi.org/10.1051/m2an/2013074

13. Vignal, P., Dalcin, L., Brown, D.L., Collier, N., Calo, V.M.: An energy-stable convex splitting for the phase-field crystal equation. Comput. Struct. **158**, 355–368 (2015). https://doi.org/10.1016/j.compstruc.2015.05.029

14. Shin, J., Lee, H.G., Lee, J.-Y.: First and second order numerical methods based on a new convex splitting for phase-field crystal equation. J. Comput. Phys. **327**, 519–542 (2016). https://doi.org/10.1016/j.jcp.2016.09.053

15. Guo, R., Xu, Y.: Local discontinuous Galerkin method and high order semi-implicit scheme for the phase field crystal equation. SIAM J. Sci. Comput. **38**(1), 105–127 (2016). https://doi.org/10.1137/15M1038803

16. Glasner, K., Orizaga, S.: Improving the accuracy of convexity splitting methods for gradient flow equations. J. Comput. Phys. **315**, 52–64 (2016). https://doi.org/10.1016/j.jcp.2016.03.042

17. Dong, L., Feng, W., Wang, C., Wise, S.M., Zhang, Z.: Convergence analysis and numerical implementation of a second order numerical scheme for the three-dimensional phase field crystal equation. Comput. Math. Appl. **75**(6), 1912–1928 (2018). https://doi.org/10.1016/j.camwa.2017.07.012

18. Diegel, A.E., Sharma, N.S.: A c^0 interior penalty method for the phase field crystal equation. Numer. Methods Partial Differ. Equ. **39**(3), 2510–2537 (2023). https://doi.org/10.1002/num.22976

19. Gomez, H., Nogueira, X.: An unconditionally energy-stable method for the phase field crystal equation. Comput. Methods Appl. Mech. Engrg. **249–252**, 52–61 (2012). https://doi.org/10.1016/j.cma.2012.03.002

20. Zhang, Z., Ma, Y., Qiao, Z.: An adaptive time-stepping strategy for solving the phase field crystal model. J. Comput. Phys. **249**, 204–215 (2013). https://doi.org/10.1016/j.jcp.2013.04.031

21. Liao, H.-L., Ji, B., Zhang, L.: An adaptive BDF2 implicit time-stepping method for the phase field crystal model. IMA J. Numer. Anal. **42**(1), 649–679 (2022). https://doi.org/10.1093/imanum/draa075

22. Park, J.-H., Null, A.J.S., Wise, S.M.: Benchmark computations of the phase field crystal and functionalized Cahn-Hilliard equations via fully implicit, nesterov accelerated schemes. Commun. Comput. Phys. **33**(2), 367–398 (2022). https://doi.org/10.4208/cicp.OA-2022-0117

23. Li, Y., Kim, J.: An efficient and stable compact fourth-order finite difference scheme for the phase field crystal equation. Comput. Methods Appl. Mech. Engrg. **319**, 194–216 (2017). https://doi.org/10.1016/j.cma.2017.02.022

24. Yang, X., Han, D.: Linearly first- and second-order, unconditionally energy stable schemes for the phase field crystal model. J. Comput. Phys. **330**, 1116–1134 (2017). https://doi.org/10.1016/j.jcp.2016.10.020

25. Liu, Z., Li, X.: Efficient modified stabilized invariant energy quadratization approaches for phase-field crystal equation. Numer. Algorithms **85**(1), 107–132 (2020). https://doi.org/10.1007/s11075-019-00804-9

26. Li, X., Shen, J.: Stability and error estimates of the SAV Fourier-spectral method for the phase field crystal equation. Adv. Comput. Math. **46**(3) (2020). https://doi.org/10.1007/s10444-020-09789-9
27. Liu, Z., Li, X.: The exponential scalar auxiliary variable (E-SAV) approach for phase field models and its explicit computing. SIAM J. Sci. Comput. **42**(3), 630–655 (2020). https://doi.org/10.1137/19M1305914
28. Lee, H.G., Shin, J., Lee, J.-Y.: First and second order operator splitting methods for the phase field crystal equation. J. Comput. Phys. **299**, 82–91 (2015). https://doi.org/10.1016/j.jcp.2015.06.038
29. Zhai, S., Weng, Z., Feng, X., He, Y.: Stability and error estimate of the operator splitting method for the phase field crystal equation. J. Sci. Comput. **86**(1) (2021). https://doi.org/10.1007/s10915-020-01386-8
30. Cao, H., Sun, Z.: Two finite difference schemes for the phase field crystal equation. Sci. China Math. **58**(11), 2435–2454 (2015). https://doi.org/10.1007/s11425-015-5025-1
31. Zhang, F., Li, D., Sun, H.-W., Zhang, J.-L.: A stabilized fully-discrete scheme for phase field crystal equation. Appl. Numer. Math. **178**, 337–355 (2022). https://doi.org/10.1016/j.apnum.2022.04.007
32. Shin, J., Lee, H.G., Lee, J.-Y.: Long-time simulation of the phase-field crystal equation using high-order energy-stable CSRK methods. Comput. Methods Appl. Mech. Engrg. **364**,(2020). https://doi.org/10.1016/j.cma.2020.112981
33. Cheng, K., Wang, C., Wise, S.M., Wu, Y.: A third order accurate in time, BDF-type energy stable scheme for the Cahn-Hilliard equation. Numer. Math. Theory Methods Appl. **15**(2), 279–303 (2022). https://doi.org/10.4208/nmtma.OA-2021-0165
34. Zhang, F., Li, D., Sun, H.-W.: Efficient and energy stable numerical schemes for the two-mode phase field crystal equation. J. Comput. Appl. Math. **427** (2023). https://doi.org/10.1016/j.cam.2023.115148
35. Swift, J., Hohenberg, P.C.: Hydrodynamic fluctuations at the convective instability. Phys. Rev. A **15**(1), 319 (1977). https://doi.org/10.1103/PhysRevA.15.319
36. Yuan, G., Yue, J., Sheng, Z., Shen, L.: The computational method for nonlinear parabolic equation (in Chinese). Sci. Sin. Math. **43**(03), 235–248 (2013). https://doi.org/10.1360/012012-616
37. Cheng, K., Wang, C., Wise, S.M.: An energy stable BDF2 Fourier pseudo-spectral numerical scheme for the square phase field crystal equation. Commun. Comput. Phys. **26**(5), 1335–1364 (2019). https://doi.org/10.4208/cicp.2019.js60.10
38. Gottlieb, S., Wang, C.: Stability and convergence analysis of fully discrete fourier collocation spectral method for 3-d viscous burgers' equation. J. Sci. Comput. **53**(1), 102–128 (2012). https://doi.org/10.1007/s10915-012-9621-8
39. Wang, C., Wise, S.M.: An energy stable and convergent finite-difference scheme for the modified phase field crystal equation. SIAM J. Numer. Anal. **49**(3), 945–969 (2011). https://doi.org/10.1137/090752675
40. Baskaran, A., Hu, Z., Lowengrub, J.S., Wang, C., Wise, S.M., Zhou, P.: Energy stable and efficient finite-difference nonlinear multigrid schemes for the modified phase field crystal equation. J. Comput. Phys. **250**, 270–292 (2013). https://doi.org/10.1016/j.jcp.2013.04.024
41. Baskaran, A., Lowengrub, J.S., Wang, C., Wise, S.M.: Convergence analysis of a second order convex splitting scheme for the modified phase field crystal equation. SIAM J. Numer. Anal. **51**(5), 2851–2873 (2013). https://doi.org/10.1137/120880677
42. Wang, M., Huang, Q., Wang, C.: A second order accurate scalar auxiliary variable (sav) numerical method for the square phase field crystal equation. J. Sci. Comput. **88**(2), 33 (2021). https://doi.org/10.1007/s10915-021-01487-y
43. Hao, Y., Huang, Q., Wang, C.: A third order bdf energy stable linear scheme for the no-slope-selection thin film model. Commun. Comput. Phys. **29**(3), 905–929 (2021). https://doi.org/10.4208/cicp.OA-2020-0074